

Manganese Abundances in Cluster and Field Stars

Jennifer S. Sobeck¹, Inese I. Ivans^{2,3}, Jennifer A. Simmerer¹, Christopher Sneden¹,
Peter Hoefflich¹, Jon P. Fulbright², and Robert P. Kraft⁴

ABSTRACT

We have derived Mn abundances for more than 200 stars in 19 globular clusters. In addition, Mn abundance determinations have been made for a comparable number of halo field and disk stars possessing an overlapping range of metallicities and stellar parameters. Our primary data set was comprised of high resolution spectra previously acquired at the McDonald, Lick and Keck Observatories. To enlarge our data pool, we acquired globular and open cluster spectra from several other investigators. Data were analyzed using synthetic spectra of the 6000 Å Mn I triplet. Hyperfine structure parameters were included in the synthetic spectra computations. Our analysis shows that for the metallicity range $-0.7 > [\text{Fe}/\text{H}] > -2.7$ stars of 19 globular clusters have a mean relative abundance of $\langle [\text{Mn}/\text{Fe}] \rangle = -0.37 \pm 0.01$ ($\sigma = 0.10$), a value in agreement with that of the field stars: $\langle [\text{Mn}/\text{Fe}] \rangle = -0.36 \pm 0.01$ ($\sigma = 0.08$). Despite the 2 orders of magnitude span in metallicity, the $\langle [\text{Mn}/\text{Fe}] \rangle$ ratio remains constant in both stellar populations. Our Mn abundance data indicate that there is no appreciable variation in the relative nucleosynthetic contribution from massive stars that undergo core-collapse supernovae and thus, no significant change of the associated initial mass function in the specified metallicity range.

Subject headings: Galaxy: abundances—Galaxy: halo—globular clusters: general—stars: abundances — stars: Population II

¹Department of Astronomy and McDonald Observatory, University of Texas, Austin, TX 78712; jsobeck@astro.as.utexas.edu, jensim@astro.as.utexas.edu, chris@verdi.as.utexas.edu, pah@astro.as.utexas.edu

²The Observatories of the Carnegie Institution of Washington, 813 Santa Barbara St., Pasadena, CA 91101; iii@ociw.edu, jfulb@ociw.edu

³Princeton University Observatory, Peyton Hall, Princeton, NJ 08544

⁴UCO/Lick Observatory, Department of Astronomy and Astrophysics, University of California, Santa Cruz, CA 95064; kraft@ucolick.org

1. INTRODUCTION

Trends in element abundances are utilized to uncover the formation patterns and evolutionary history of the Galaxy. Comparison of chemical compositions between different stellar populations is essential to this endeavor. The interconnection between halo field and globular cluster stars is of extreme interest since their metallicity ranges overlap (e.g. Laird et al. 1988, and references therein). Recent general overviews of abundance trends in halo populations have been done by, e.g., McWilliam (1997) and Gratton et al. (2004).

With the exception of ω Cen (e.g. Norris & Da Costa 1995), stars of individual globular clusters display monometallicity, i.e. members of a globular cluster possess approximately the same $[\text{Fe}/\text{H}]$ value. Elements of the proton-capture group (C, N, O, Na, Mg, and Al) exhibit large star-to-star abundance variations in most globular clusters, and these discrepancies are inordinately large as compared to those seen in halo field stars (Gratton et al. 2004, and references therein). In contrast, members of the α -element (like Si, Ca, and Ti) and neutron-capture element (like Y, Ba, La, and Eu) groups display similar abundance patterns in most globular cluster and halo field stars. Likewise, the relative abundances of several Fe-peak elements (notably Sc, V, Cr, and Ni) appear to be almost identical in the two stellar populations. The vast majority of the Fe-group members have roughly solar abundance ratios with two exceptions: copper and manganese. The relative abundance of Cu is known to be exceedingly subsolar in metal-poor field stars (at metallicities $[\text{Fe}/\text{H}] < -2$, $[\text{Cu}/\text{Fe}]$ approaches -1 ; Sneden et al. 1991a, Mishenina et al. 2002). An analogous deficiency of Cu in globular cluster stars has recently been reported by Simmerer et al. (2003). In the two stellar groups, the trend of $[\text{Cu}/\text{Fe}]$ with $[\text{Fe}/\text{H}]$ is identical within the limit of observational uncertainty.

Mn also has an established abundance deficiency in metal-poor stars. Helfer et al. (1960) and Wallerstein (1962) were the first to report sub-solar Mn and in 1978, Beynon verified these initial observations. Later, Gratton (1989) improved Mn abundance determinations by employing hyperfine structure (HFS) data from Booth et al. (1984) to derive $\langle [\text{Mn}/\text{Fe}] \rangle = -0.34 \pm 0.06$ for stars of metallicity $[\text{Fe}/\text{H}] < -1$. Three factors have hindered Mn abundance determinations: the lack of adequate hyperfine structure computations, the uncertainty of damping parameter values, and the absence of available transitions in the red portion of the visible spectrum (Gratton 1989; Prochaska & McWilliam 2000). Several surveys of metal-poor field stars have derived highly accurate $[\text{Mn}/\text{Fe}]$ values (Gratton & Sneden 1991; McWilliam et al. 1995; Johnson 2002; Francois et al. 2003; Cohen et al. (2004b)). However, a systematic and comprehensive study of Mn abundances in globular cluster stars has not yet taken place.

In this paper we present Mn abundances for several hundred cluster and field stars in

the metallicity range of $0.0 \gtrsim [\text{Fe}/\text{H}] \gtrsim -2.7$. Our intent is two-fold: first, we want to ascertain whether globular cluster stars have the same Mn abundance as stars of the halo field; and second, we wish to confirm the Mn abundance trend across the entire metallicity spectrum, as well as across the stellar populations, in order to further resolve the nucleosynthetic origin of this element. In §2 we relay particulars about each data set and characterize the general nature of the data. A justification of line selection and a description of the analysis is found in §3. An account of all abundance values is given in §4. Finally in §5, a discussion of these Mn results ensues.

2. OBSERVATIONS AND DATA REDUCTION

In this study, Mn abundance measurements were made in three stellar populations: globular clusters, open clusters, and the halo field. Spectroscopic and equivalent width data were acquired from numerous sources. A significant portion of the globular cluster and halo field data were gathered by the Lick-Texas group (LTG). These LTG data constitute a basis set for our Mn abundance survey. Table 1 lists the relevant observational parameters and literature sources for the LTG data. Cluster sample size varies from as few as 2 to as many as 23 stars. The two field star surveys each have a sample size in excess of 80 stars. Stars in the field data sample exist in a variety of evolutionary states whereas the bulk of the globular cluster data are red giants. Three facilities were used for the LTG observations: the Keck I 10.0 m telescope equipped with the High Resolution Echelle Spectrometer (HIRES; Vogt et al. 1994), the Lick 3.0 m telescope equipped with the Hamilton spectrograph (Vogt 1987), and the McDonald 2.7 m telescope equipped with the “2d-coudé” spectrograph (Tull et al. 1995). For the various instrument configurations, the resolution ($R \equiv \lambda/\Delta\lambda$) ranges from 30,000 to 60,000, and the estimated signal-to-noise ratio (S/N) varies between 25 and 180. The software packages IRAF¹ and SPECTRE (Fitzpatrick & Sneden 1987) were used for standard data reduction processes such as bias and flat-field correction, order extraction, cosmic ray elimination, continuum adjustment, and wavelength correction.

The remainder of the globular and open cluster spectra were obtained from several external sources. Data contributors, as well as observational details, are found in Table 2. These data were collected at several facilities: the Very Large Telescope (VLT), Apache Point Observatory (APO), Cerro Tololo Inter-American Observatory (CTIO), and Keck.

¹IRAF is distributed by the National Optical Astronomy Observatories, which are operated by the Association of Universities for Research in Astronomy, Inc., under cooperative agreement with the National Science Foundation.

The various telescope-spectrograph combinations yielded resolutions of $24,000 \leq R \leq 60,000$ and S/N values between 30 and 135. A variety of data reduction and analysis programs were used by the contributors, and for further details the reader should consult the original references (as listed in Table 2).

3. ANALYSIS

Line selection was based on metallicity and effective temperature parameters. A considerable number of the globular cluster and halo field stars in the data sample have $T_{\text{eff}} \leq 4850$. Accordingly, analysis of the strong Mn lines at 4030 Å and 4823 Å was not feasible due to the flux constraints of the data and the probable saturation of these features. In addition, most extant cluster spectra do not extend to the blue-violet wavelength region.

To ascertain Mn abundance in these stars, a wavelength range of 6000-6030 Å was chosen, which encompasses three Mn I spectral features at 6013.51, 6016.64, and 6021.82 Å. These lines are the sole strong transitions of Mn in the yellow-red spectral regime. Two Fe lines at 6024.06 and 6027.05 Å which are roughly of the same excitation potential as the Mn features, were employed for a local iron abundance determination. The use of these nearby Fe transitions eliminates possible discrepancies in continuous opacity and issues with regard to first-order continuum placement. And although the convenience of these two lines must not be understated (as they lie on the same spectral order as the three Mn features), our goal was to obtain local [Fe/H] values for the [Mn/Fe] determination, not to replace the more extensive [Fe/H] assessments done in previous LTG studies. Figure 1 features all of the lines used for analysis and roughly illustrates line strength as a function of metallicity.

3.1. Model Atmospheres and Techniques

For the LTG data, we adopted the stellar atmospheric parameters as reported by the original papers. We employed the model stellar atmospheres that were generated for those papers from the MARCS (Gustaffson et al. 1975) and ATLAS (Kurucz 1993) codes. Table 3 presents the T_{eff} , v_t , and $\log g$ numbers for the LTG data set. Model atmospheres did not normally accompany the data from outside sources. We took the stellar atmospheric parameters as reported by the contributors and generated the models for these quantities from the grid of ATLAS models without convective overshoot (Castelli et al. 1997) using software originally provided by A. McWilliam. Table 4 displays the parameters for the stars of the external source data set.

In order to refine the line list, we synthesized a portion of the solar spectrum (6000-6030 Å). The observed center-of-disk photospheric spectrum is that of Delbouille et al. (1990)². We selected a Holweger-Müller model with a microturbulent velocity of $v_t = 0.80 \text{ km s}^{-1}$, a value in accord with other solar abundance surveys (Holweger & Müller 1974; Grevesse & Sauval 1999). We used the standard LTG value of $\log\epsilon(\text{Fe})_{\odot} = 7.52$ as set by Sneden et al. (1991b). The initial basis for this value originates from the work of Anders & Grevesse (1989). Further confirmation of this value was done by Anstee et al. (1997), who used neutral iron lines to derive an iron abundance for the Sun of 7.51 ± 0.01 . Several other studies arrive at approximately the same value (to within 0.1 dex) for the solar photospheric abundance of iron (e.g. Raassen & Uylings 1998; Asplund et al. 2000). We also adopt $\log\epsilon(\text{Mn})_{\odot} = 5.39$ as recommended by Anders & Grevesse (1989). Note, however, that there is a significant discrepancy between the solar photospheric and meteoritic CI chondrite [$\log\epsilon(\text{Mn})_{\text{meteor}} = 5.50$; Lodders 2003] values for Mn.

Spectrum synthesis was employed to determine the abundances as accurate determinations from transitions with multiple HFS components necessitate this technique. Abundance derivations that rely solely on the measurement of equivalent width values do not properly account for lines containing HFS without the introduction of an artifact (i.e., an arbitrary increase in microturbulent velocity; Cohen 1978). To generate synthetic spectra and to calculate abundances, the current version of the LTE line analysis code MOOG (Sneden 1973) was used. The raw relative flux values generated by this code were convolved with Gaussian broadening functions to reproduce the combined effects of astrophysical (i.e. macroturbulence) and instrumental (i.e. spectrograph slit) origin. Figure 2 shows a sample spectrum synthesis. In cases in which the spectra were not available, we employed literature values of the equivalent width measurements. In those instances we computed synthetic spectrum fluxes, which were then summed to force-fit the observed equivalent width values. This technique was verified in some spectra for which synthetic fits were also made to observed spectra.

3.2. Line Parameters

Two Fe I features (6024 and 6027 Å) are available for abundance determinations in the specified wavelength range. A reliable Fe abundance may be obtained from these neutral lines as their excitation potential is large ($\chi > 4.0 \text{ eV}$); consequently, they are not as susceptible

²We employed the electronic version available on the website of the Base de données Solaire Sol, <http://bass2000.obspm.fr/home.php>

to temperature effects and departures from LTE (Grevesse et al. 1996). Multiple literature sources give a transition probability for the 6027 Å feature. The emission measurement technique of O’Brian et al. (1991) yielded a gf-value for the 6027 Å line that is in good agreement with that found by the absorption line technique of Blackwell et al. (1982) . We adopted the O’Brian et al. log (gf) value for this line.

Unfortunately, neither O’Brian et al. (1991) nor Blackwell et al. (1982) give a transition probability for the 6024 Å feature. Literature sources for this line include the early work of Wolnik et al. (1970), $\log(\text{gf}) = -0.06 \pm 0.00$; the solar line inversion value of Thévenin (1990), $\log(\text{gf}) = -0.02 \pm 0.02$; and the semi-empirical derivation of Kurucz (1993), $\log(\text{gf}) = -0.120$. Taking into consideration the lack of modern laboratory atomic physics input into these numbers, we opted to perform an empirical derivation of the 6024 Å gf-value. An initial line list (in the specified 30 Å wavelength range) was assembled from Kurucz (1993) data. A synthetic spectrum was generated from this list and compared to the observed solar spectrum. Modification of the line list (i.e. revision of gf-values and deletion of non-essential features) occurred until the difference between the observed spectrum and the synthetic spectrum was minimized. With the refined line list in place, the iterative determination of the 6024 Å gf-value proceeded. The abundances of Mn and Fe were set to their corresponding solar values and the smoothing and continuum were fixed. Then the transition probability and the van der Waals damping parameter (C6) of the 6024 Å line were allowed to vary until a good fit was achieved. A final value of $\log(\text{gf})_{6024} = 0.04$ was obtained, with associated enhancement of the C6 damping parameter of $E\gamma = 2.2$. The result for the damping parameter enhancement is in agreement with the finding of Anstee et al. (1997 and references therein) that lines with an excitation potential greater than 3.0 eV generally have an $E\gamma > 2.1$.

With a nuclear spin of $I = 5/2$ and a magnetic dipole moment of $\mu_I = 3.4687 \mu_N$ (Lederer & Shirley 1978), Mn has a sizable HFS. The effect of HFS is to desaturate and broaden the lines of Mn. The strongest transitions of Mn are particularly susceptible. To ensure the accurate computation of Mn abundance, HFS was taken into account. Oscillator strengths for the 6013 and 6021 Å Mn lines were taken from Booth et al. (1983, 1984). Additional data were acquired from the Kurucz (1993) line list. Neither Booth et al. (1983) nor the NIST database ³ (Martin et al. 1999) give a transition probability for the 6016 Å line. As before, the gf value for the 6016 Å Mn line was determined iteratively via a fit to the observed solar spectrum. Notably, the 6016 line possesses a significant Fe contaminant, whereas the 6013 and 6021 Å features do not contain any prominent blends. So, little weight is accorded to the abundance derived from the 6016 Å feature due to line contamination and

³The associated NIST website is: <http://physics.nist.gov/PhysRefData/ASD/index.html>.

slight uncertainty in oscillator strength value (it is used for a consistency check only). Final transition probabilities for all lines are reported in Table 5.

4. RESULTS

Our essential finding is that in the metallicity range $-0.7 > [\text{Fe}/\text{H}] > -2.7$ the Mn abundances in globular cluster stars are equivalent to those of halo field stars. Figure 3 displays the $[\text{Mn}/\text{Fe}]$ ratio as a function of $[\text{Fe}/\text{H}]$ for all data. The mean abundance in the specified metallicity range is $\langle [\text{Mn}/\text{Fe}] \rangle = -0.37 \pm 0.01$ ($\sigma = 0.10$) for globular cluster stars and $\langle [\text{Mn}/\text{Fe}] \rangle = -0.36 \pm 0.01$ ($\sigma = 0.08$) for halo field stars. Figure 4 presents the correlation of S/N with $[\text{Mn}/\text{Fe}]$ for the LTG data set. As shown in the bottom panel, very high S/N data ($\text{S/N} > 175$) give an extremely consistent $[\text{Mn}/\text{Fe}]$ value. In Figure 5 the scatter in $[\text{Mn}/\text{Fe}]$ is shown for selected globular clusters with large data samples. Intra-cluster variations with respect to Mn abundance are nominal, and scatter is within observational error. However, our chosen Fe features contribute to scatter in Fe, as demonstrated in Figure 6. In a few cases the spread in metallicity is larger than 0.3 dex. The inclusion of more Fe lines (of both ionization states) would somewhat improve the abundance determination. So for the LTG clusters, we list our $[\text{Fe}/\text{H}]$ values, as well as our $[\text{Fe}/\text{H}]$ ratios averaged with those reported by the original reference. Table 6 presents the $[\text{Fe}/\text{H}]$ and $[\text{Mn}/\text{Fe}]$ values that result from this averaging process. In the designated $[\text{Fe}/\text{H}]$ range, we were able to obtain from the literature $[\text{Mn}/\text{Fe}]$ data points for five globular clusters: M55, M68, NGC 104, M71, and M30. These literature $[\text{Mn}/\text{Fe}]$ values are in fairly good agreement with our own. A few clusters in our sample were a bit problematic, and we discuss these clusters in the following sections. We also address the noticeable data gaps in the extremely-poor metallicity range ($[\text{Fe}/\text{H}] < -2.7$ dex) and the slightly-metal poor range ($[\text{Fe}/\text{H}] > -0.7$ dex) in section §4.4.

4.1. Error Analysis

Four main factors contribute to possible errors in our abundances: choice of model, sensitivity to stellar parameters, quality of observational data, and modification of elements of the spectral fit process. To assess the ramifications of model/parameter variation across the entire data set, we studied representative stars of three metallicity classes: slightly metal-poor (SMP), moderately metal-poor (MMP), and extremely metal-poor (EMP). The selection of the stellar atmosphere model (be it MARCS or Kurucz) seemed to have little effect on either $[\text{Mn}/\text{H}]$ or $[\text{Fe}/\text{H}]$ (with a maximum change of 0.07 dex in $[\text{Fe}/\text{H}]$ for a SMP star). The relative abundances are not very responsive to slight changes in the stellar

parameters. For a change of ± 100 K in T_{eff} , the largest effect was seen in the $[\text{Fe}/\text{H}]$ (± 0.10 dex) of SMP stars. An alteration in the $\log g$ value of ± 0.20 dex had a maximum response in the $[\text{Fe}/\text{H}]$ of EMP stars with a change of ± 0.10 dex. The $[\text{Mn}/\text{H}]$ value responded similarly, but taken together in the ratio $[\text{Mn}/\text{Fe}]$ the effect cancels out. And for $\Delta v_t = \pm 0.20 \text{ km s}^{-1}$, the greatest change is seen in EMP stars with ± 0.09 dex in both $[\text{Mn}/\text{H}]$ and $[\text{Fe}/\text{H}]$. Overall, the abundance error from the variation of these stellar parameters does not exceed ± 0.10 dex.

The S/N across the entire data set did vary by a substantial amount: $25 \leq \text{S/N} \leq 180$. For data of generally high quality ($\text{S/N} > 75$), the abundance determined via spectral synthesis fit is good to within ± 0.05 dex. Conversely, the fit for low quality data is not as solid and may fluctuate by as much as ± 0.10 dex. Further considerations are continuum normalization and smoothing parameters of the fit. Placement of the continuum might affect the fit by as much as ± 0.03 dex, whereas alteration of the FWHM of the fitting function (normally a Gaussian for most stars) may result in an abundance change of roughly ± 0.05 dex.

Non-LTE effects should also be taken into consideration. For metal-poor stars, overionization (and its impact on surface gravity) is indeed a factor (Thevenin & Idiart 1999), but to what degree is not clear (Kraft & Ivans 2003; Korn 2004). To date, no non-LTE Mn abundance calculations have been published for stars of any type. In a survey of metal-poor giants, Johnson (2002) attempted to quantify the effect on Mn by estimating a non-LTE $\log g$. Johnson demonstrated that modification of the $\log g$ value elicited a change of roughly -0.10 dex in Mn abundance. Ivans et al. (2001) suggest that as long as the abundance ratio consists of two neutral species (as is the case in our study) the relative non-LTE effects are minimized.

4.2. M71

Our initial result for M71 indicated a high Mn abundance as compared to other globular clusters in our data sample. For 10 stars, we derived $\langle [\text{Mn}/\text{Fe}] \rangle = -0.16$ ($\sigma = 0.14$) with an average metallicity of $\langle [\text{Fe}/\text{H}] \rangle = -1.12$ ($\sigma = 0.15$). The data have an unusually large scatter in both Mn and Fe. We must take into consideration the fact that our M71 observational runs at the Lick 3.0 m telescope occurred in 1989 and 1991, prior to the update of the echelle spectrograph. If we discount the four most anomalous data points (which correspond to the lowest S/N values), then the $\langle [\text{Fe}/\text{H}] \rangle$ for M71 becomes -1.04 ($\sigma = 0.12$) and the $\langle [\text{Mn}/\text{Fe}] \rangle$ is -0.26 ($\sigma = 0.08$). Also, if we average our $[\text{Fe}/\text{H}]$ ratios with those reported in the original LTG M71 study, then $\langle [\text{Fe}/\text{H}] \rangle = -0.91$ ($\sigma = 0.06$) and $\langle [\text{Mn}/\text{Fe}] \rangle = -0.38$ ($\sigma = 0.11$). With regard to these considerations, the M71 abundances are much more in line

with other data points of similar metallicity. Using Keck I data acquired in 2002, Ramirez & Cohen were able to ascertain Mn abundances for M71. For this cluster, they derive $\langle[\text{Fe I}/\text{H}]\rangle = -0.71 \pm 0.08$ and $\langle[\text{Mn}/\text{Fe}]\rangle = -0.27 \pm 0.11$. Due to the higher resolution and S/N of the Ramirez & Cohen (2002) data, their abundance values are to be preferred (Figure 3, bottom).

4.3. Comparison of Cluster Results: NGC 6528 and C261

We are able to compare our derived $[\text{Mn}/\text{Fe}]$ ratios to literature values for two clusters of high metallicity, NGC 6528 and Collinder 261 (Cr 261). NGC 6528 presents an opportunity to study the cluster populations of the Galactic Bulge. It lies in Baade’s window and thus has only moderate reddening. Although Cr 261 is an open cluster, it may be likened to globular clusters, as it is similar in age (roughly 9 Gyr; Janes & Phelps (1994)).

For three red horizontal branch stars of NGC 6528, Carretta et al. (2001) found $\langle[\text{Fe I}/\text{H}]\rangle = 0.07$ ($\sigma = 0.02$) and $\langle[\text{Mn}/\text{Fe}]\rangle = -0.37$ ($\sigma = 0.07$). In our examination of three different stars from this cluster, we derive mean values of $\langle[\text{Fe}/\text{H}]\rangle = -0.24$ ($\sigma = 0.19$) and $\langle[\text{Mn}/\text{Fe}]\rangle = -0.25$ ($\sigma = 0.06$). As Zoccali et al. (2004) have pointed out in their study of NGC 6528, factors that affect abundance derivations include effective temperature assessment (both spectroscopically and photometrically derived parameters contain inherent errors) and continuum determination (placement of the continuum may be largely variable due to the presence of molecular bands and α enhancement). Our Fe values for this cluster do show a large spread: $-0.37 \leq [\text{Fe}/\text{H}] \leq -0.03$ (the temperature range of the sample stars is a likely factor). Also, special attention should be paid to the broadening factors used in abundance determination (Zoccali et al. 2004). While taking into consideration all the issues mentioned above, we remark that we still find a substantial underabundance of Mn in NGC 6528.

Carretta et al. (2005) also observed six red clump and red giant branch stars in Cr 261. For this cluster, they found $\langle[\text{Fe I}/\text{H}]\rangle = -0.03$ ($\sigma = 0.04$) and $\langle[\text{Mn}/\text{Fe}]\rangle = -0.03$ ($\sigma = 0.04$). We employed a different data set (Friel et al. 2003) that contains four of the stars that were in the Carretta et al. (2005) sample. Our analysis of Cr 261 giants yields $\langle[\text{Fe}/\text{H}]\rangle = -0.36$ ($\sigma = 0.21$) and $\langle[\text{Mn}/\text{Fe}]\rangle = -0.32$ ($\sigma = 0.13$). Data concerns might include instrument resolution and S/N values. Moreover, there is definite sensitivity in the data to the selection of v_t , transition probabilities, and $\log g$ values (Carretta et al. 2005). We note that there is significant scatter in our Fe abundance, and it is indeed a rather low value. In both studies, one target star gave consistently low $[\text{Fe}/\text{H}]$ and $[\text{Mn}/\text{Fe}]$ values as compared to other stars in the data set. None of the studies chose to exclude this star (most

likely due to the small data sample for Cr 261). These are preliminary investigations of clusters in the metallicity regime $[\text{Fe}/\text{H}] > -0.70$ and the acquisition of more data in this range will be necessary. Future efforts will also focus on open cluster abundances.

4.4. Other Mn Abundance Analyses

Several investigations of the Mn abundance ratio have been done in various metallicity regimes and stellar populations. We briefly detail some of those here along with the associated $[\text{Mn}/\text{Fe}]$ results. For field stars of low metallicity ($[\text{Fe}/\text{H}] < -1.7$), Johnson (2002) obtained a subsolar Mn abundance. Studies by Cohen et al. (2004) and Francois et al. (2003) find that Mn decreases steadily below metallicity $[\text{Fe}/\text{H}] \sim -3.0$.

Examinations of Mn in metal-rich field stars are plentiful in the literature. Solar neighborhood stars in the range $-0.15 < [\text{Fe}/\text{H}] < 0.45$ have been found by Chen et al. (2003) to possess a relatively constant $[\text{Mn}/\text{Fe}]$ ratio hovering roughly at zero. Alternatively, the solar neighborhood survey of Allende Prieto et al. (2004) reported that $[\text{Mn}/\text{Fe}]$ rises in step with $[\text{Fe}/\text{H}]$. Mn abundance determinations of the disk field stars include Feltzing & Gustafsson (1998), Prochaska et al. (2000b), and Reddy et al. (2003). Generally, these studies find that as $[\text{Fe}/\text{H}]$ approaches zero, so, accordingly, does the Mn abundance with respect to Fe (with the rough determination of the solar Mn abundance level at solar metallicity). In addition, these studies report that above $[\text{Fe}/\text{H}] = 0$, increases in $[\text{Fe}/\text{H}]$ correspond to attendant increases in $[\text{Mn}/\text{Fe}]$. E. Carretta et al. (2006, in preparation) have conducted Mn abundance analyses of several open clusters. They have found that the open clusters of their data sample do mimic the trend of the disk. Now, Prochaska et al (2000) contend that Mn abundance differs between the thick disk and the thin disk. They conclude that Mn in the thick disk is normally underabundant with respect to the thin disk. This finding is being subjected to further scrutiny (Reddy et al. 2006).

Bulge globular clusters have not been well analyzed and remain somewhat of a mystery (the notable exception, of course, being NGC 6528). McWilliam et al. (2003) have discovered that the $[\text{Mn}/\text{Fe}]$ values of bulge giants follow the trend of disk stars. In a separate study, McWilliam et al. (2003) examined the $[\text{Mn}/\text{Fe}]$ ratio in the Sagittarius dwarf spheroidal galaxy and found a fairly consistent underabundance with respect to the stars of the bulge and disk populations. In order to have a more complete view of these metal-rich stellar populations, further study is requisite.

5. DISCUSSION AND CONCLUSIONS

We have derived Mn abundances for hundreds of globular cluster, open cluster, and halo field stars. We used spectral synthesis in order to obtain a $[\text{Fe}/\text{H}]$ and $[\text{Mn}/\text{Fe}]$ ratio for each star. In the range $-0.7 > [\text{Fe}/\text{H}] > -2.7$, globular cluster stars exhibit a mean relative abundance of $\langle [\text{Mn}/\text{Fe}] \rangle = -0.37 \pm 0.01$ ($\sigma = 0.10$), which is the same (to within the levels of uncertainty) as that of halo field stars, $\langle [\text{Mn}/\text{Fe}] \rangle = -0.36 \pm 0.01$ ($\sigma = 0.08$). There is no statistically significant difference with regard to Mn abundance between the halo field and globular clusters.

Figure 7 displays the average abundance ratios of Fe-peak elements in halo field and globular cluster stars in the metallicity range $-0.7 > [\text{Fe}/\text{H}] > -2.7$. Several points may be gleaned from this plot. First, and most important, the elemental abundance ratios are equivalent in the two stellar populations. Second, the relative abundances for many members of the Fe group (Sc, V, Cr, Co, and Ni) are roughly solar over this metallicity range. And third, the abundances of a few odd Z-numbered elements (namely, Mn and Cu) are deficient with respect to their even Z-numbered Fe-peak counterparts.

Nucleosynthesis of Mn occurs primarily via decay of ^{55}Co (Nakamura et al. 1999). Another possible nucleosynthetic pathway for Mn is α -capture by ^{51}V . The main site for Mn formation is the incomplete explosive Si-burning region (Nakamura et al. 1999). In the metallicity range of interest ($-0.7 > [\text{Fe}/\text{H}] > -2.7$), core-collapse supernovae (SNe) are predominantly responsible for the production of Mn. Yields of Mn rely heavily upon the neutron excess (Umeda & Nomoto 2002). The $[\text{Mn}/\text{Fe}]$ ratio depends on the mass cut (as Fe has two production sites: the incomplete and complete Si-burning regions) and the explosion energy (with little dependence on stellar mass; Umeda & Nomoto 2002).

The single-valued $[\text{Mn}/\text{Fe}]$ ratio in the range $-0.7 > [\text{Fe}/\text{H}] > -2.7$ may be described as a plateau (Figure 3). Though the metallicity changes by roughly a factor of 100, $\langle [\text{Mn}/\text{Fe}] \rangle$ does not vary in either globular cluster or halo field stars. In the specified range, the $[\text{Mn}/\text{Fe}]$ ratio of (either stellar population) is not metallicity-dependent. These data indicate that the contribution from stars that undergo core collapse SNe (i.e., medium to moderately high mass stars) is uniform and does not change. Furthermore, the data suggest that the initial mass function (IMF) associated with these stars is essentially invariant. As Thielemann et al. (1996) contend, in the range $-1.0 \geq [\text{Fe}/\text{H}] \geq -2.5$, constant abundance ratios of elements (like those of the Fe peak) should be expected as the core collapse SNe of the entire mass range of progenitor stars occurs.

Beyond $[\text{Fe}/\text{H}] \sim -1.0$, there is an increase in the $[\text{Mn}/\text{Fe}]$ scatter for the field star data points, and the relative Mn abundance rises steadily as solar metallicity is approached

(Figure 3). A possible explanation for the increase in scatter is that in this metallicity regime stars of three populations are present (halo, thin disk, and thick disk). Notably, Reddy et al. (2006) present data that show no difference in the Mn abundance between the stars of the thin and thick disk (of the same metallicity). The emergence of Type Ia SN events is likely responsible for the observable increase in the levels of Mn. This follows as the production of Mn occurs mostly in Type Ia SNe (e.g., Samland 1998; Iwamoto et al. 1999).

It would be advantageous to use the $[O/Mn]$ ratio in the examination of the evolution of very massive stars (the highest end of the IMF). Virtually all synthesis of O occurs in massive stars. The full extent of the mass range of core collapse progenitors produces Fe (Thielemann et al. $\sigma = 0.10$) 1996). Mn differs from Fe in that its manufacture occurs in a wide but limited portion of that mass range for Type II SNe. Consequently, the $[O/Mn]$ ratio could provide constraints on the uppermost portion of the IMF. Unfortunately, as it pertains to this discussion, significant star-to-star variation of O abundance occurs in evolved stars of globular clusters with the diminution of O being due to the CNO and NeNa cycles of H burning (the proton-capture reactions; Denissenkov & Weiss 2004; Gratton et al. 2004). As the bulk of the current study data is from globular cluster stars, little about nucleosynthesis in massive stars would be learned from $[O/Mn]$ correlations. Work on this issue should be pursued with large field star samples that are extremely metal-poor ($[Fe/H] < -3.0$) or metal-rich ($[Fe/H] > -0.5$) in nature.

Few recent theoretical reviews of elemental yields and abundances in the metallicity range of interest, $-0.7 > [Fe/H] > -2.7$, have been published. The comprehensive investigation by Timmes et al. (1995) examined the chemical evolution of 76 stable isotopes in this range using the output from the Type II SN models of Woosley & Weaver (1995). Timmes et al. found excellent agreement between their calculations and the observational data for Cr and Ni. Although the trends for Mn, Sc, and V were well reproduced, the calculations of Timmes et al. predicted systematically lower abundance values for these elements than those found by observation. The trend for Cu was fairly well duplicated, although the actual values for the calculated abundance were quite low in contrast to observational values. The disagreement between theoretical calculations and observational results widens as the extremely low metallicity regime is considered. Limongi & Chieffi (2005) compared their yields from zero metallicity core collapse SNe to the extremely metal-poor star data of Cayrel et al. (2004). The observational data for the abundance ratios of the Fe-peak elements could not be simultaneously reproduced by any of the models (regardless of the choice of mass cut). This discrepancy encourages the continued development of theoretical calculations.

Further elucidation of the metal-rich regime is necessary, with special emphasis paid to bulge and disk clusters. It must be determined whether NGC 6528 is unique in its

chemical evolution history (as suggested by McWilliam & Rich 2004) or, indeed, whether it is representative of all bulge clusters. In addition, verification of the Mn abundance trend in the IR wavelength range and extension of this study to metal rich candidates is paramount. It would also be valuable to re-investigate Fe-peak elements such as Co and Sc with large abundance uncertainties.

We wish to thank to E. Carretta for many informative and insightful discussions. We would like to acknowledge the data contributions of these investigators: J. Cohen, E. Friel, G. Gonzalez, F. Grundahl, J. W. Lee, M. Shetrone, and M. Zoccali. We are deeply indebted to them. We are grateful to the following agencies for providing funding support for this research: NASA, through Hubble Fellowship grant HST-HF-01151.01-A from the Space Telescope Science Institute, operated by AURA, Inc., under NASA contract NAS 5-26555 to I. I. I.; and the NSF, through grants AST 03-07495 to C. S. and AST 00-98453 to R. P. K.

REFERENCES

- Allende Prieto, C., Barklem, P. S., Lambert, D. L., & Cunha, K. 2004, *Å*, 420, 183
- Anders, E., & Grevesse, N. 1989, *Geochim. Cosmochim. Acta*, 53, 197
- Anstee, S.D., O'Mara, B. J., & Ross, J. E. 1997, *MNRAS*, 284, 202
- Asplund, M., Nordlund, A., Trampedach, R., & Stein, R. F. 2000, *A&A*, 359, 743
- Beynon, T. G. R. 1978, *A&A*, 64, 145
- Blackwell, D. E., Petford, A. D., Shallis, M. J., & Simmons, G. J. 1982, *MNRAS*, 199, 43
- Booth, A. J., Shallis, M. J., & Wells, M. 1983, *MNRAS*, 205, 191
- Booth, A. J., Blackwell, D. E., & Shallis, M. J. 1984, *MNRAS*, 209, 77
- Carretta, E., Cohen J. G., Gratton, R. G. & Behr, B. B. 2001, *AJ*, 122, 1469
- Carretta, E., Bragaglia, A., Gratton, R.G., & Tosi, M. 2005, *Å*, 441, 131
- Caretta, E. et al. 2006, in preparation
- Castelli, F., Gratton, R. G., & Kurucz, R. L. 1997, *Å*, 318, 841
- Cayrel, R., Depagne, E., Spite, M., Hill, V., Spite, F., Francois, P., Plez, B., Beers, T., Primas, F., Andersen, J., Barbuy, B., Bonifacio, P., Molaro, P., & Nordstrom, B. 2004, *A&A*, 416, 1117
- Chen, Y. Q., Zhao, G., Nissen, P. E., Bai, G. S., & Qiu, H. M. 2003, *ApJ*, 591, 925
- Cohen, J. G. 1978, *ApJ*, 223, 487
- Cohen, J. G. 2004a, *AJ*, 127, 1545
- Cohen, J. G., Christlieb, N., McWilliam, A., Shectman, S., Thompson, I., Wasserburg, G. J., Ivans, I. I., Dehn, M., Karlsson, T., & Melendez, J. 2004b, *ApJ*, 612, 1107
- Delbouille, L., Roland, G., & Neven, L. 1990, Liege: Universite de Liege Institut d'Astrophysique
- Denissenkov, P. A. & Weiss, A. 2004, *ApJ*, 603, 119
- Feltzing, S., & Gustafsson, B. 1998, *A&AS*, 129, 237

- Fitzpatrick, M. J. & Sneden, C. 1987, BAAS, 19, 1129
- Francois, P., Depagne, E., Hill, V., Spite, M., Spite, F., Plez, B., Beers, T. C., Barbuy, B., Cayrel, R., Andersen, J., Bonifacio, P., Molaro, P., Nordström, B., & Primas, F. 2003, A&A, 403, 1105
- Friel, E. D., Jacobson, H. R., Barrett, E., Fullton, L., Balachandran, S. C., & Pilachowski, C. 2003, AJ, 126, 2372
- Fulbright, J. P. 2000, AJ, 120, 1841
- Gonzalez, G., & Wallerstein, G. 1998, AJ, 116, 765
- Gonzalez, G., & Wallerstein, G. 2000, PASP, 112, 1081
- Gratton, R. G. 1989, A&A, 208, 171
- Gratton, R. G., & Sneden, C. 1991, A&A, 241, 501
- Gratton, R. G., Carretta, E., Claudi, R., Lucatello, S., & Barbieri, M. 2003, A&A, 404, 187
- Gratton, R. G., Sneden, C., & Carretta, E. 2004, ARA&A, 42, 385
- Grevesse, N., Noels, A., & Sauval, A. J. 1996 Astronomical Society of the Pacific Conference Series; volume 99 edited by Stephen S. Holt and George Sonneborn, p.117
- Grevesse, N., & Sauval, A. J. 1999, A&A, 347, 348
- Grundahl, F., Briley, M., Nissen, P. E., & Feltzing, S. 2002, A&A, 385, L14
- Gustafsson, B., Bell, R. A., Eriksson, K. & Nordlund, A. 1975, A&A, 42, 407
- Helfer, H. L., Wallerstein, G., & Greenstein, J. L. 1960, ApJ, 132, 553
- Holweger, H., & Mueller, E.A., 1974, Sol. Phys., 39, 19
- Ivans, I. I., Sneden, C., Kraft, R. P., Suntzeff, N. B., Smith, V. V., Langer, G. E. & Fulbright, J. P. 1999, AJ, 118, 1273
- Ivans, I. I., Kraft R. P., Sneden, C., Smith, G. H., Rich, R. M. , & Shetrone, M. 2001, AJ, 122, 1438
- Iwamoto, K., Brachwitz, F., Nomoto, K., Kishimoto, N., Umeda, H., Hix, W. R., & Thielemann, F. K. 1999, ApJS, 125, 439

- Janes, K. A., & Phelps, R. L. 1994, *AJ*, 108, 1773
- Johnson, J. A. 2002, *ApJS*, 139, 219
- Korn, A. J. 2004, *Carnegie Centennial Symposium: Origin and Evolution of the Elements*
- Kraft, R. P., Sneden, C., Langer, G. E., Shetrone, M. D., & Bolte, M. 1995, *AJ*, 109, 2586
- Kraft, R. P., Sneden, C., Smith, G. H., Shetrone, M. D., Langer, G. E., & Pilachowski, C. A. 1997, *AJ*, 113, 279
- Kraft, R. P., Sneden, C., Smith, G. H., Shetrone, M. D. & Fulbright, J. 1998, *AJ*, 115, 1500
- Kraft, R. P., & Ivans, I. I. 2003, *PASP*, 115, 143
- Kurucz, R. L. 1993, *Kurucz CD-ROM 13, ATLAS 9* (Cambridge:SAO)
- Laird, J. B., Rupen, M. P., Carney B. W., & Latham, D. W. 1988, *AJ*, 96, 1908
- Lederer, M. C., & Shirely, V. S. 1978, *Table of Isotopes*, 7th ed. (New York: Wiley)
- Lee, J. W., & Carney, B. W. 2002, *AJ*, 124, 1511
- Limongi, M., & Chieffi, A. 2005,
- Lodders, K. 2003, *AJ*, 591, 1220
- Martin, W. C., Fuhr, J. R. Kelleher, D. E., Musgrove, A., Sugar J., Wiese, W. L., Mohr, P. J., & Olsen, K. 1999, *NIST Atomic Spectra Database, Version 2.0* (Gaithersburg: NIST)
- McWilliam, A., Preston, G. W., Sneden, C., & Searle, L. 1995, *AJ*, 109, 2757
- McWilliam, A. 1997, *ARA&A*, 35, 503
- McWilliam, A., Rich, M. R., & Smecker-Hane, T. A. 2003, *ApJ*, 592, L21
- McWilliam, A., & Rich, M. R. 2004, *Carnegie Centennial Symposium: Origin and Evolution of the Elements*
- Mishenina, T. V., Kovtyukh, V. V., Soubraïn, C., Travaglio, C., & Busso, M. 2002, *A&A*, 396, 189
- Nakamura, T., Umeda, H., Nomoto, K., Thielmann, F. K., & Burrow, A. 1999, *ApJ*, 517, 193

- Norris, J. E., & Da Costa, G. S. 1995, *ApJ*, 447, 680
- O’Brian, T. R., Wickliffe, M. E., Lawler, J. E., Whaling, W., & Brault, J. W. 1991, *J. Opt. Soc. Am. B*, 8, 1185
- Prochaska, J. X., & McWilliam, A. 2000, *ApJ*, 537, 57
- Prochaska, J. X., Naumov, S. O., Carney, B. W., McWilliam, A., & Wolfe, A. M. 2000, *AJ*, 120, 2513
- Raassen, A. J. J., & Uylings, P. H. M. 1998, *A&A*, 340, 300
- Ramirez, S. V., & Cohen, J. G. 2002, *ApJ*, 123, 3277
- Reddy, B. E., Tomkin, J., Lambert, D. L., & Allende Prieto, C. 2003, *MNRAS*, 340, 304
- Reddy, B. E., Lambert, D. L., & Allende Prieto, C. 2006, *MNRAS*, submitted
- Samland, M. 1998, *ApJ*, 496, 155
- Shetrone, M. D., Bolte, M., & Stetson, P. B. 1998, *AJ*, 115, 1888
- Shetrone, M. D., & Keane, M. J. 2000, *AJ*, 119, 840
- Simmerer, J. A., Sneden, C., Ivans, I. I., Kraft, R. P., Shetrone, M. D., & Smith, V. V. 2003, *AJ*, 125, 2018
- Simmerer, J. A., Sneden, C., Cowan, J. J., Collier, J., Woolf, V. M., & Lawler, J. E. 2004, *ApJ*, 617, 1091
- Smith, G. H., Sneden, C., & Kraft, R. P. 2002, *AJ*, 123, 1502
- Sneden, C. 1973, *ApJ*, 184, 839
- Sneden, C., Gratton, R. G., & Crocker, D. A. 1991a, *A&A*, 246, 354
- Sneden, C., Kraft, R. P., Prosser, C. F., & Langer, G. E. 1991b, *AJ*, 102, 2001
- Sneden, C., Kraft, R. P., Langer, G. E., Prosser, C. & Shetrone, M. 1994, *AJ*, 107, 1773
- Sneden, C., Kraft, R. P., Shetrone, M. D., Smith, G. H., Langer, G. E., & Prosser, C. F. 1997 *AJ*, 114, 1964
- Sneden, C., Kraft, R. P., Prosser, C. F., & Langer, G. E. 1991, *AJ*, 102, 2001

- Sneden, C., Kraft, R. P., Guhathakurta, P., Peterson, R., & Fulbright, J. P. 2004, *AJ*, 127, 2162
- Thevenin, F. 1990, *A&AS*, 82, 179
- Thevenin, F., & Idiart, T. P. 1999, *ApJ*, 521, 753
- Thielemann, F. K., Nomoto, K., & Hashimoto, M. 1996, *ApJ*, 460, 408.
- Timmes, F. X., Woosley, S. E., & Weaver, T. A. 1995, *ApJS*, 98, 617
- Tull, R. G., MacQueen, P. J., Sneden, C., & Lambert, D. L. 1995, *PASP*, 107, 251
- Umeda, H. & Nomoto, K. 2002, *ApJ*, 565, 385
- Vogt, S. S. 1987, *PASP*, 99, 1214
- Vogt, S. S. et al. 1994, *Proc. SPIE*, 2198, 362
- Wallerstein, G. 1962, *ApJS*, 6, 407
- Wolnik, S. J., Berthel, R. O., & Wares, G. W. 1970, *ApJ*, 162, 1037
- Woosely, S. E., & Weaver, T. A. 1995, *ApJS*, 101, 181
- Yong, D., Grundahl, F., Nissen, P. E., Jensen, H. R., & Lambert, D. L. 2005, *A&A*, 438, 875
- Zoccali, M., Barbuy, B., Hill, V., Ortolani, S., Renzini, A., Bica, E., Momany, Y., Pasquini, L., Minniti, D., & Rich, R. M. 2004, *A&A*, 423, 507

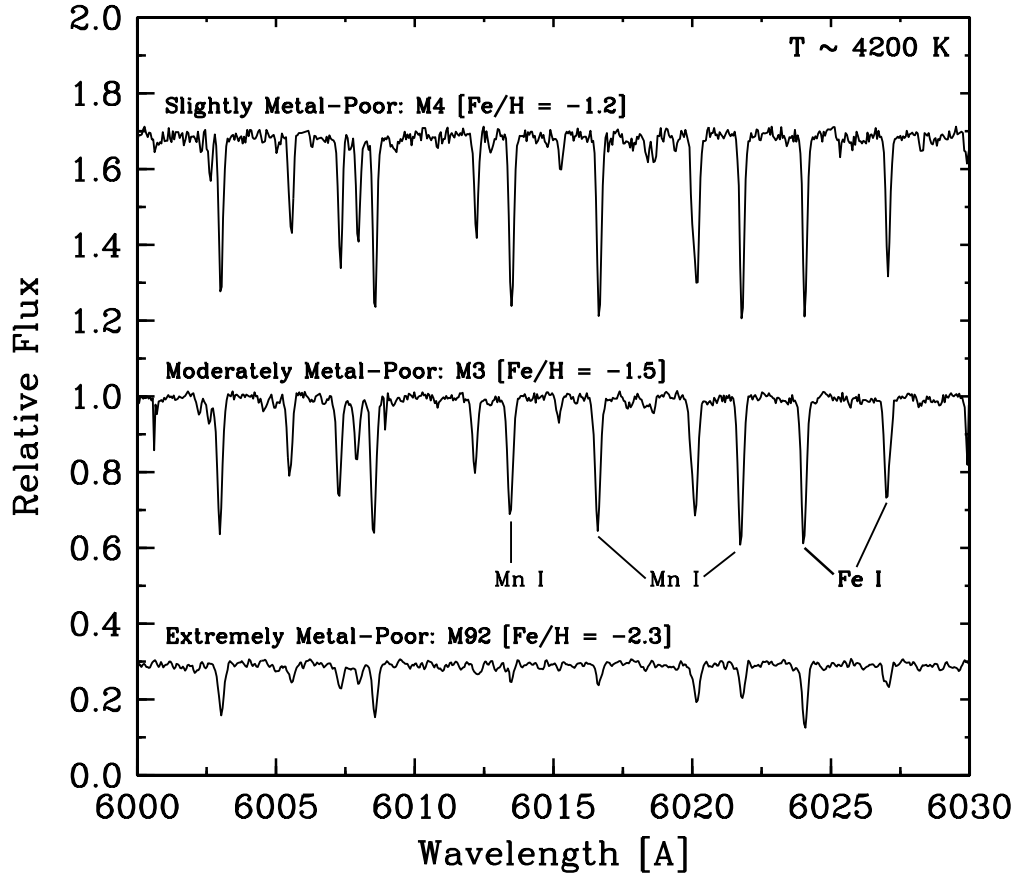


Fig. 1.— Comparison of the spectra from globular clusters of differing metallicities. Note that temperature is roughly the same for all of the spectra. The three Mn and two Fe lines used in the abundance analysis are indicated in this figure. As metallicity decreases, some of the spectral features become undetectable.

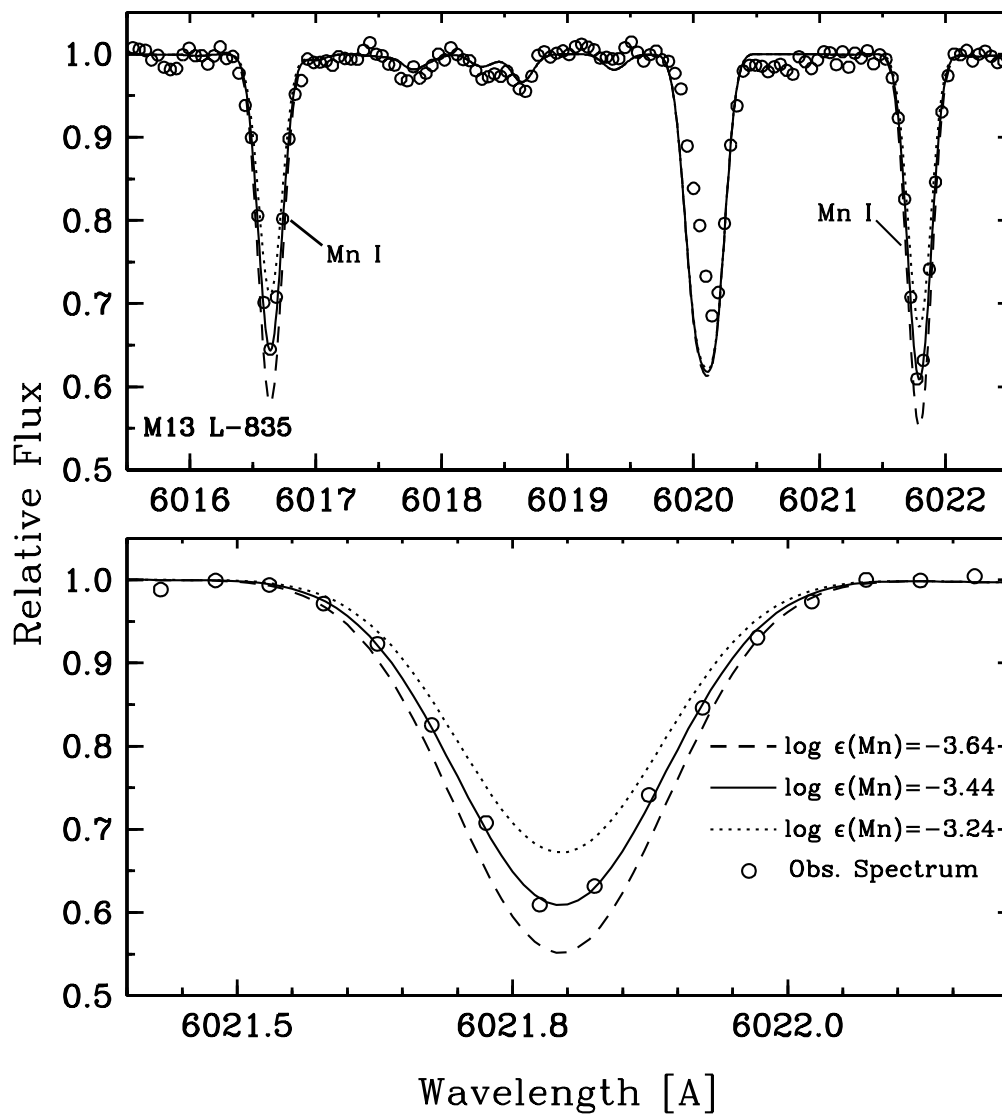


Fig. 2.— Comparison of the synthetic and observed spectrum for one M13 star. The top panel displays the observed and synthetic spectra for a wavelength range that encompasses the 6016 and 6021 Å Mn lines. The bottom panel focuses on the 6021 Å Mn feature and highlights the effects of incremental changes in abundance. Changes as small as 0.2 dex cause distinct variation in the synthesized spectrum.

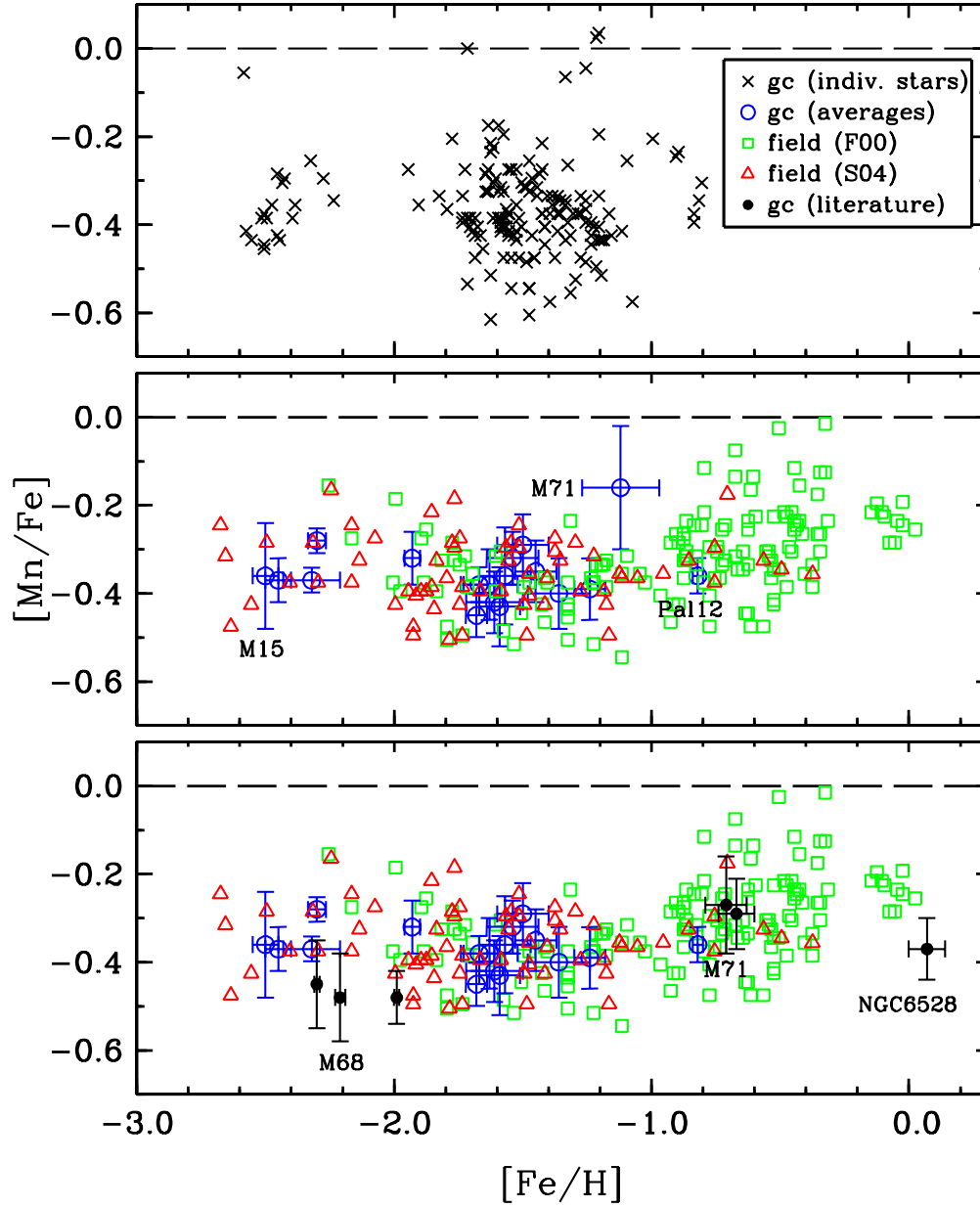


Fig. 3.— Correlation of $[\text{Mn}/\text{Fe}]$ with $[\text{Fe}/\text{H}]$ for different stellar samples. The top panel displays all of the abundances for the stars of the 19 globular cluster data sample. The middle panel shows the average $[\text{Mn}/\text{Fe}]$ and $[\text{Fe}/\text{H}]$ values for each globular cluster (with associated error bars). Field star abundances are also shown in this panel; label F00 indicates data from Fulbright (2000) and label S04 signifies data from Simmerer et al. (2004). The points for M15 and Pal 12 are designated as they represent the extremes in metallicity for the halo globular clusters of this data set. Moreover, M71 is denoted as its $\langle [\text{Mn}/\text{Fe}] \rangle$ is not consistent with the other globular cluster data points. The bottom panel presents globular cluster values from the literature. Note that the literature Mn abundances agree fairly well with those of the current study. Also, the Mn abundance for M71 from the current data sample is set aside in favor of the value published by Ramirez & Cohen (2002), as explained in §4.2.

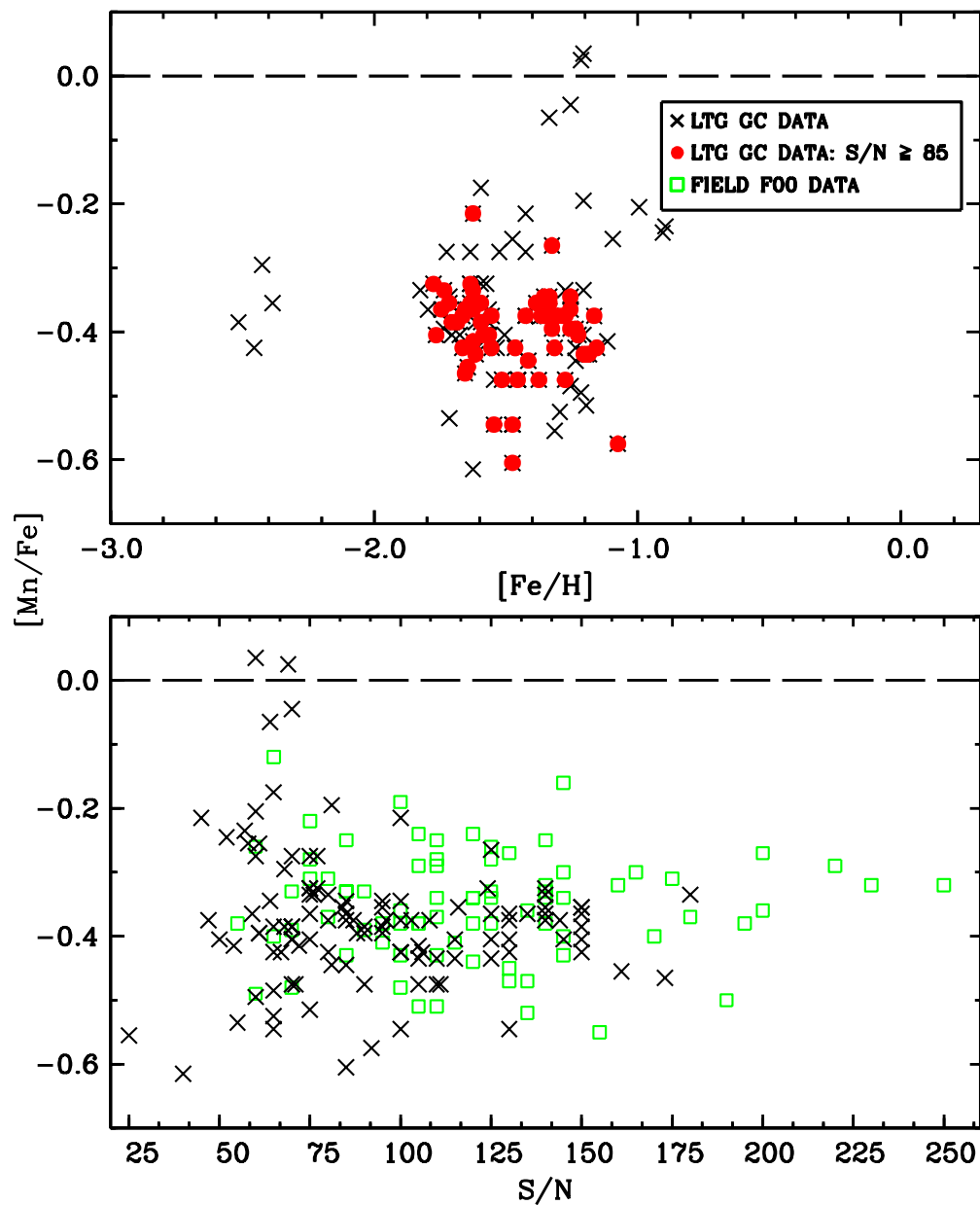


Fig. 4.— Interdependence of $[\text{Mn}/\text{Fe}]$ and S/N for the LTG data sample. The top panel presents the entire S/N range of the LTG globular cluster data set as well as those points with $S/N > 85$. The bottom panel illustrates the correlation of Mn abundances with S/N for LTG globular cluster and field data in the metallicity range $-0.7 > [\text{Fe}/\text{H}] > -2.7$.

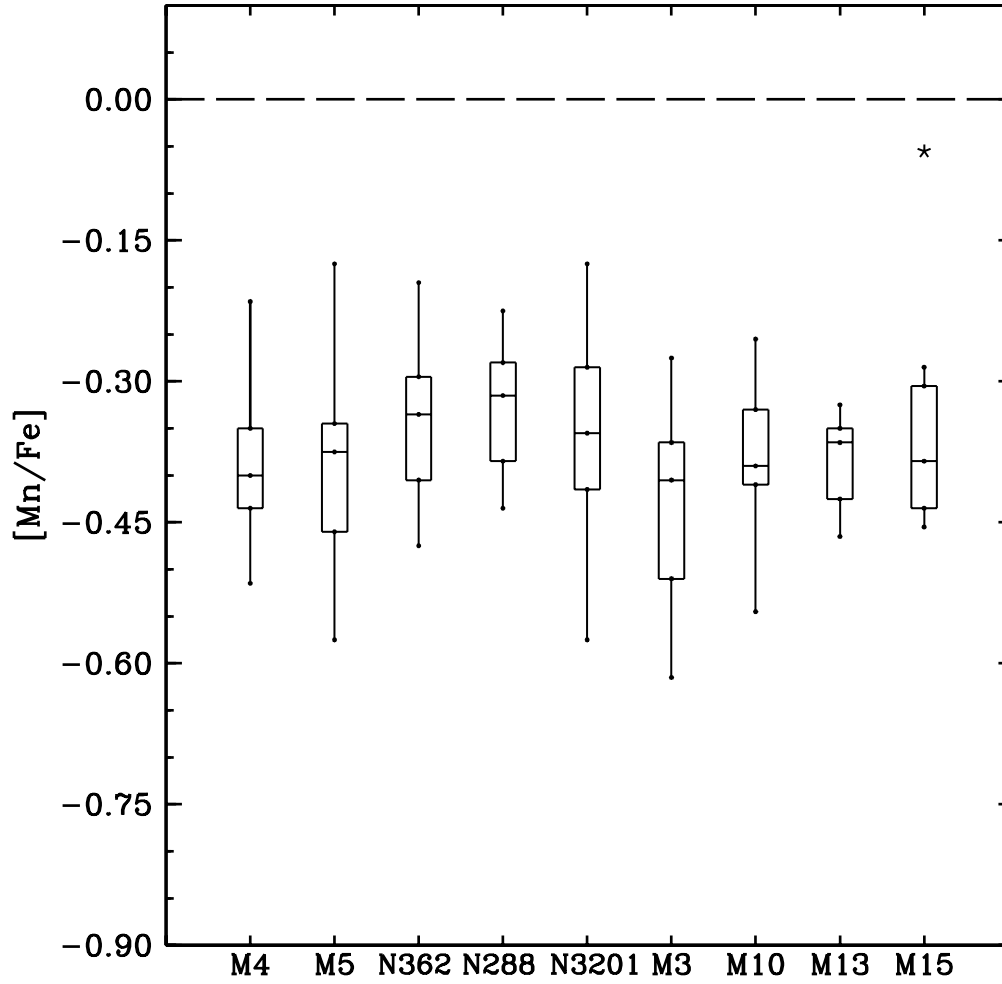


Fig. 5.— Box plots for nine representative globular clusters. For each cluster, the boxed region encompasses the interquartile (middle 50%) of its [Mn/Fe] data. Also featured are the median (horizontal line), range (vertical lines; excludes outliers), and outliers (an outlier has a value greater than 1.5 times the interquartile range). The ordering of the clusters is in decreasing $[\text{Fe}/\text{H}]_{\text{avg}}$.

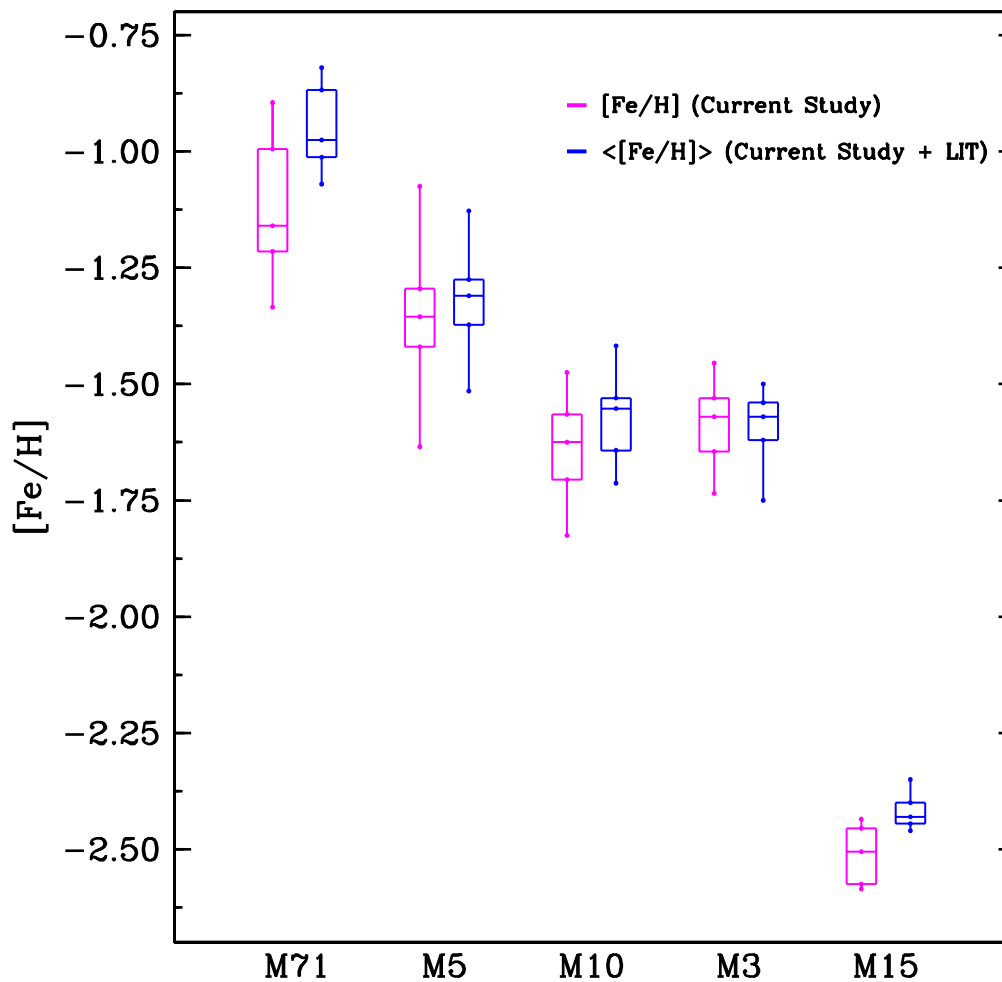


Fig. 6.— Box plots for selected globular clusters. For a few cases, averaging our derived $[\text{Fe}/\text{H}]$ values with those reported in the literature serves to reduce the spread in metallicity. As a consequence of this averaging process, the median $[\text{Fe}/\text{H}]$ value for the cluster increases. In general, marginal benefit is gained from the averaging process (as clearly illustrated by M3).

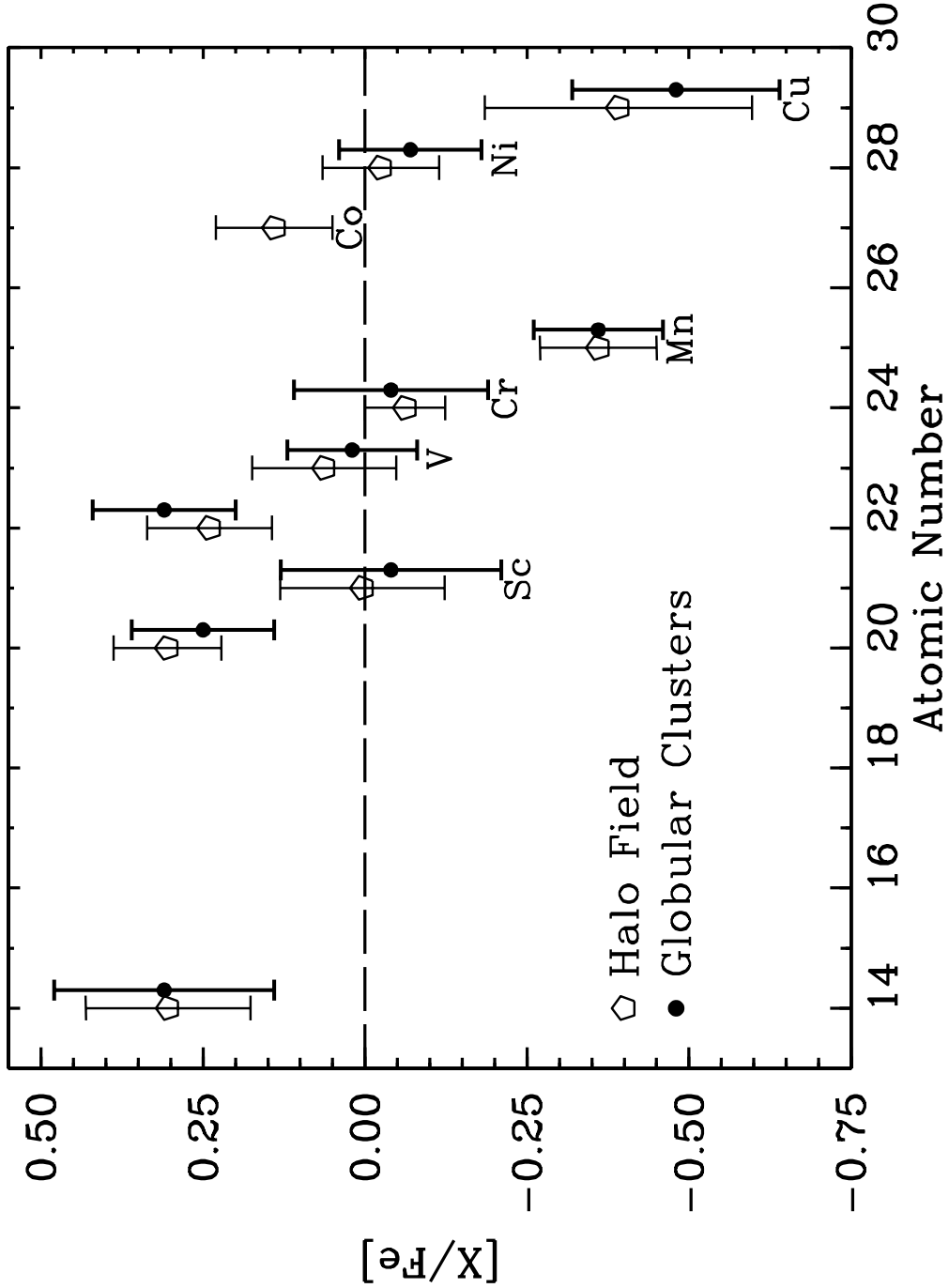


Fig. 7.— Average abundance ratios with associated standard deviation values for some of the Fe-peak and α -elements in the range $-0.7 > [\text{Fe}/\text{H}] > -2.7$. Globular cluster data are obtained from the LTG references. The Mn values are provided by the current study. Data for halo field stars for every element except Cu and Co are taken from Gratton et al. (2003) and Fulbright (2000). Cu field star data are obtained from Mishenina et al. (2002) and Co field star data are taken from Johnson (2002). Interestingly, there is a lack of Co data for globular clusters. Note that in almost every case, the average values for globular cluster and halo field stars are roughly equal to one another.

Table 1. LTG Observational Data

Cluster	Program Stars ^a	Instrument ^b	Reference ^c	S/N Range ^d
NGC 5272 (M3)	20	Keck(45)	1	40-150 D
NGC 5904 (M5)	8	Lick(30)	2	25-145 A
	23	Keck(45)		
NGC 6121 (M4)	20	McD(30:60)	3	40-170 B
NGC 6205 (M13)	17	Lick(30)	4	65-180 A
NGC 6254 (M10)	12	Lick(30)	5	60-180 A
NGC 6341 (M92)	4	Keck(45)	6	60-85 A
NGC 6838 (M71)	10	Lick(30)	7	55-85 A
NGC 7006	6	Keck(45)	8	55-95 B
NGC 7078 (M15)	5	Keck(45)	9	75-150 C
	6	Lick(50)		
Pal 5	4	Keck(34)	10	60-100 B
Halo Field Survey	130	Lick(50)	11	40-240 F
	*	Keck(45)		
	*	ESO (40)		
Halo Field Survey	86	McD(60)	12	\simeq 100 E

^aNote that the number of program stars does not always equal those found in the original paper. In some cases, the S/N ratio was too low in specified wavelength range to obtain a [Mn/Fe] ratio.

^bESO (50): ESO 3.6m telescope-CASPEC spectrograph with $R \simeq 40,000$; Keck(34), Keck (45): Keck I 10.0m telescope-HIRES spectrograph with $R \simeq 34,000$ or $R \simeq 45,000$; Lick(30): Pre-1995 configuration of Lick 3.0m telescope-Hamilton echelle with $R \simeq 30,000$; Lick(50): Current configuration of Lick 3.0m telescope-Hamilton echelle with $R \simeq 50,000$; McD(30-60): McDonald 2.7m telescope-”2d-coudé” with $R \simeq 30,000$ or $R \simeq 60,000$.

^c(1) Sneden et al. 2004. (2) Ivans et al. 2001. (3) Ivans et al. 1999. (4) Kraft et al. 1997. (5) Kraft et al. 1995. (6) Shetrone et al. 1998. (7) Sneden et al.

1994. (8) Kraft et al. 1998. (9) Sneden et al. 1997. (10) Smith et al. 2002. (11) Fulbright 2000. (12) Simmerer et al. 2004.

^dApproximate S/N at A: 6300 Å; B: 6350 Å; C: 6363 Å; D: 6460 Å; E: 4100 Å; F: 5500 Å.

Table 2. Outside Source Cluster Observational Data

Cluster	Program Stars ^a	Instrument ^b	Reference ^c	S/N Range ^d
Cr 261	4	CTIO(30)	1	75-100
NGC 288	13	CTIO(30)	2	60-125 B
NGC 362	12	CTIO(30)	2	70-95 B
NGC 3201	14	CTIO(30)	3	40-70 C
NGC 6287	2	CTIO(30)	4	≈95
NGC 6293	2	CTIO(30)	4	95~100
NGC 6528	3	VLT	5	30-40
NGC 6541	2	CTIO(30)	4	95~135
NGC 6705 (M11)	6	CTIO(24)	6	85-130
	4	APO(34)		
NGC 6752	4	VLT(40:60)	7, 8	≈100 B
Pal 12	4	Keck(34)	9	>100 A

^aNote that the number of program stars does not always equal those found in the original paper. In some cases, the S/N ratio was too low in specified wavelength range to obtain a [Mn/Fe] ratio.

^bKeck(34): Keck I 10.0m telescope-HIRES spectrograph with $R \simeq 34,000$; CTIO(24), CTIO(30): CTIO 4.0m telescope-echelle spectrograph with $R \simeq 24,000$ or $R \simeq 30,000$; VLT(40:60): VLT telescope-UVES spectrograph with $R \simeq 40,000$ or $R \simeq 60,000$; APO(34): APO 3.5m telescope-echelle spectrograph with $R \simeq 34,000$.

^c(1) Friel et al. 2003. (2) Shetrone & Keane 2000. (3) Gonzalez & Wallerstein 1998. (4) Lee & Carney 2002. (5) Zoccali et al. 2004. (6) Gonzalez & Wallerstein 2000. (7) Grundahl et al. 2002. (8) Yong et al. 2005. (9) Cohen 2004a.

^dApproximate S/N at A: 5865 Å; B: 6700 Å; C: 7500 Å

Table 3. LTG Stellar Model Parameters and Individual [Fe/H] and [Mn/Fe] Values

Association	Star	T_{eff} (K)	log g	v_t (km s ⁻¹)	[Fe/H] LIT ^a	[Fe/H]	[Mn/Fe]
NGC 5272 (M3)	B21	4725	1.65	1.20	-1.61	-1.48	-0.61
NGC 5272 (M3)	B23	4800	2.10	1.40	-1.70	-1.63	-0.61
NGC 5272 (M3)	B24	4450	1.00	1.90	-1.59	-1.52	-0.48
NGC 5272 (M3)	B33	4550	1.30	1.65	-1.55	-1.48	-0.55
NGC 5272 (M3)	B34	3850	0.00	2.00	-1.62	-1.55	-0.55
NGC 5272 (M3)	B11	4400	1.10	1.50	-1.56	-1.59	-0.41
NGC 5272 (M3)	B12	4400	1.10	1.80	-1.62	-1.74	-0.34
NGC 5272 (M3)	B13	3900	0.00	2.05	-1.54	-1.58	-0.41
NGC 5272 (M3)	B14	4175	0.70	1.70	-1.58	-1.60	-0.39
NGC 5272 (M3)	B15	4350	1.10	1.50	-1.67	-1.67	-0.43
NGC 5272 (M3)	B41	4075	0.40	1.70	-1.54	-1.57	-0.41
NGC 5272 (M3)	B42	4100	0.40	1.70	-1.56	-1.56	-0.43
NGC 5272 (M3)	B43	4750	1.40	1.60	-1.75	-1.71	-0.39
NGC 5272 (M3)	B44	5050	2.00	1.50	-1.71	-1.71	-0.41
NGC 5272 (M3)	B45	5100	2.40	1.00	-1.58	-1.73	-0.28
NGC 5272 (M3)	F24	4600	1.70	1.20	-1.54	-1.51	-0.41
NGC 5272 (M3)	I21	4175	0.70	1.70	-1.52	-1.57	-0.39
NGC 5272 (M3)	IV-101	4200	0.75	1.70	-1.50	-1.46	-0.48
NGC 5272 (M3)	IV-77	4300	0.85	1.80	-1.52	-1.60	-0.33
NGC 5272 (M3)	VZ1397	3925	0.10	2.00	-1.53	-1.57	-0.37
NGC 5904 (M5)	G2	3900	-0.10	1.75	-1.33	-1.38	-0.48
NGC 5904 (M5)	I-14	4250	0.75	1.60	-1.34	-1.36	-0.38
NGC 5904 (M5)	I-2	4500	1.10	1.45	-1.31	-1.29	-0.38
NGC 5904 (M5)	I-20	4050	0.00	2.00	-1.44	-1.60	-0.18
NGC 5904 (M5)	I-50	4525	1.15	1.40	-1.33	-1.28	-0.48
NGC 5904 (M5)	I-55	4700	0.85	1.80	-1.47	-1.56	-0.38
NGC 5904 (M5)	I-58	4350	0.80	1.50	-1.27	-1.34	-0.35
NGC 5904 (M5)	I-61	4400	1.00	1.50	-1.32	-1.36	-0.35
NGC 5904 (M5)	I-68	4066	0.63	2.20	-1.44	-1.45	-0.58
NGC 5904 (M5)	I-71	4360	1.12	1.65	-1.32	-1.38	-0.37

Table 3—Continued

Association	Star	T_{eff} (K)	log g	v_t (km s ⁻¹)	[Fe/H] LIT ^a	[Fe/H]	[Mn/Fe]
NGC 5904 (M5)	II-50	4525	1.15	1.35	-1.24	-1.31	-0.38
NGC 5904 (M5)	II-59	4463	1.15	1.65	-1.33	-1.32	-0.56
NGC 5904 (M5)	II-74	4525	1.30	1.30	-1.17	-1.08	-0.58
NGC 5904 (M5)	II-85	4009	0.54	1.80	-1.30	-1.37	-0.31
NGC 5904 (M5)	III-122	4001	0.44	2.00	-1.26	-1.23	-0.54
NGC 5904 (M5)	III-18	4475	0.55	1.70	-1.43	-1.42	-0.45
NGC 5904 (M5)	III-3	4076	0.63	1.95	-1.31	-1.41	-0.41
NGC 5904 (M5)	III-36	4227	0.91	1.65	-1.28	-1.28	-0.47
NGC 5904 (M5)	III-52	4625	1.50	1.45	-1.38	-1.39	-0.36
NGC 5904 (M5)	III-53	4700	1.05	1.75	-1.52	-1.64	-0.33
NGC 5904 (M5)	III-59	4575	1.20	1.35	-1.30	-1.24	-0.45
NGC 5904 (M5)	III-78	4154	0.78	1.95	-1.32	-1.38	-0.45
NGC 5904 (M5)	IV-19	4125	0.50	1.70	-1.39	-1.32	-0.43
NGC 5904 (M5)	IV-26	4650	1.05	1.40	-1.41	-1.43	-0.38
NGC 5904 (M5)	IV-30	4625	1.00	1.75	-1.47	-1.47	-0.43
NGC 5904 (M5)	IV-34	4275	0.65	1.55	-1.28	-1.33	-0.40
NGC 5904 (M5)	IV-36	4575	1.50	1.35	-1.27	-1.28	-0.38
NGC 5904 (M5)	IV-4	4625	1.55	1.20	-1.24	-1.40	-0.38
NGC 5904 (M5)	IV-47	4110	0.50	1.85	-1.34	-1.30	-0.53
NGC 5904 (M5)	IV-59	4229	0.79	2.10	-1.40	-1.44	-0.45
NGC 5904 (M5)	IV-81	3945	0.00	1.90	-1.35	-1.37	-0.38
NGC 6121 (M4)	1408	4525	1.30	1.70	-1.18	-1.23	-0.41
NGC 6121 (M4)	1411	3950	0.60	1.65	-1.21	-1.26	-0.35
NGC 6121 (M4)	1514	3875	0.35	1.95	-1.23	-1.34	-0.36
NGC 6121 (M4)	1701	4625	1.50	1.65	-1.20	-1.20	-0.44
NGC 6121 (M4)	2206	4325	1.35	1.55	-1.18	-1.21	-0.34
NGC 6121 (M4)	2208	4350	1.40	1.70	-1.12	-1.17	-0.38
NGC 6121 (M4)	2307	4075	0.85	1.45	-1.20	-1.28	-0.34
NGC 6121 (M4)	2406	4100	0.45	2.45	-1.22	-1.26	-0.40
NGC 6121 (M4)	3207	4700	1.65	1.70	-1.18	-1.21	-0.44

Table 3—Continued

Association	Star	T_{eff} (K)	log g	v_t (km s ⁻¹)	[Fe/H] LIT ^a	[Fe/H]	[Mn/Fe]
NGC 6121 (M4)	3209	3975	0.60	1.75	-1.22	-1.26	-0.37
NGC 6121 (M4)	3215	4775	1.40	1.85	-1.17	-1.24	-0.43
NGC 6121 (M4)	3413	4175	1.20	1.65	-1.18	-1.33	-0.27
NGC 6121 (M4)	3612	4250	1.10	1.45	-1.20	-1.21	-0.41
NGC 6121 (M4)	3624	4225	1.10	1.45	-1.16	-1.24	-0.40
NGC 6121 (M4)	4201	4450	1.35	1.85	-1.19	-1.19	-0.44
NGC 6121 (M4)	4302	4775	1.45	1.80	-1.18	-1.22	-0.50
NGC 6121 (M4)	4511	4150	1.10	1.55	-1.16	-1.16	-0.43
NGC 6121 (M4)	4513	5250	1.00	1.65	-1.20	-1.43	-0.22
NGC 6121 (M4)	4611	3725	0.30	1.70	-1.16	-1.20	-0.52
NGC 6121 (M4)	4613	3750	0.20	1.65	-1.19	-1.26	-0.49
NGC 6205 (M13)	L-629	3950	0.20	2.00	-1.68	-1.72	-0.36
NGC 6205 (M13)	II-90	4000	0.30	2.00	-1.60	-1.65	-0.46
NGC 6205 (M13)	II-67	3950	0.20	2.10	-1.58	-1.65	-0.37
NGC 6205 (M13)	I-48	3920	0.30	2.00	-1.60	-1.66	-0.47
NGC 6205 (M13)	L-598	3900	0.00	2.10	-1.64	-1.67	-0.38
NGC 6205 (M13)	IV-22	4700	1.90	1.50	-1.56	-1.63	-0.37
NGC 6205 (M13)	II-9	4700	1.70	1.50	-1.59	-1.63	-0.42
NGC 6205 (M13)	II-28	4850	1.75	2.00	-1.68	-1.78	-0.33
NGC 6205 (M13)	IV-25	4000	0.15	2.25	-1.61	-1.64	-0.37
NGC 6205 (M13)	L-835	4090	0.55	1.90	-1.56	-1.63	-0.34
NGC 6205 (M13)	I-54	4975	1.70	1.75	-1.71	-1.77	-0.41
NGC 6205 (M13)	I-72	4850	1.90	1.45	-1.65	-1.75	-0.37
NGC 6205 (M13)	II-1	4850	2.10	1.25	-1.58	-1.62	-0.44
NGC 6205 (M13)	I-12	4600	1.50	1.60	-1.58	-1.66	-0.37
NGC 6205 (M13)	IV-19	4650	1.50	1.60	-1.59	-1.64	-0.36
NGC 6205 (M13)	II-41	4750	2.00	1.75	-1.51	-1.60	-0.36
NGC 6205 (M13)	III-52	4335	1.00	2.00	-1.54	-1.72	-0.35
NGC 6254 (M10)	A-I-2	3975	0.00	2.10	-1.47	-1.64	-0.33
NGC 6254 (M10)	A-I-60	4400	1.10	1.60	-1.53	-1.48	-0.55

Table 3—Continued

Association	Star	T_{eff} (K)	$\log g$	v_t (km s ⁻¹)	[Fe/H] LIT ^a	[Fe/H]	[Mn/Fe]
NGC 6254 (M10)	A-I-61	4550	1.00	2.00	-1.69	-1.74	-0.40
NGC 6254 (M10)	A-II-24	4050	0.10	2.00	-1.50	-1.55	-0.48
NGC 6254 (M10)	A-III-16	4150	0.90	2.00	-1.52	-1.62	-0.39
NGC 6254 (M10)	A-III-21	4060	0.50	2.10	-1.49	-1.64	-0.28
NGC 6254 (M10)	A-III-5	4400	1.20	1.75	-1.36	-1.48	-0.26
NGC 6254 (M10)	C	4200	0.75	2.00	-1.66	-1.80	-0.37
NGC 6254 (M10)	D	4200	1.05	2.00	-1.50	-1.59	-0.40
NGC 6254 (M10)	E	4350	0.80	2.00	-1.61	-1.83	-0.34
NGC 6254 (M10)	H-I-15	4225	0.75	1.75	-1.52	-1.59	-0.42
NGC 6254 (M10)	H-I-367	4135	0.60	1.70	-1.54	-1.68	-0.41
NGC 6341 (M92)	III-13	4180	0.10	2.15	-2.24	-2.39	-0.36
NGC 6341 (M92)	III-65	4260	0.30	1.80	-2.25	-2.46	-0.43
NGC 6341 (M92)	VII-122	4300	0.70	1.85	-2.32	-2.52	-0.39
NGC 6341 (M92)	VII-18	4220	0.20	2.00	-2.27	-2.43	-0.30
NGC 6838 (M71)	A4	4100	0.80	2.25	-0.78	-1.34	-0.07
NGC 6838 (M71)	I	4300	1.00	2.00	-0.89	-1.26	-0.05
NGC 6838 (M71)	1-77	4100	0.95	2.00	-0.78	-1.22	0.03
NGC 6838 (M71)	1-45	4050	0.80	2.00	-0.76	-1.21	-0.20
NGC 6838 (M71)	1-53	4300	1.40	2.00	-0.79	-1.21	0.04
NGC 6838 (M71)	1-113	3950	0.70	2.00	-0.85	-1.12	-0.42
NGC 6838 (M71)	1-46	4000	0.80	2.15	-0.77	-1.10	-0.26
NGC 6838 (M71)	S	4300	1.25	2.00	-0.72	-1.00	-0.21
NGC 6838 (M71)	1-21	4350	1.45	2.00	-0.73	-0.91	-0.25
NGC 6838 (M71)	A9	4200	1.20	2.00	-0.85	-0.90	-0.24
NGC 7006	I-1	3900	0.10	2.25	-1.55	-1.72	-0.39
NGC 7006	II-103	4200	0.75	1.85	-1.55	-1.58	-0.33
NGC 7006	II-18	4300	0.90	1.85	-1.56	-1.46	-0.48
NGC 7006	II-46	4200	0.50	2.25	-1.60	-1.54	-0.43
NGC 7006	V19	4100	0.30	2.40	-1.62	-1.69	-0.39
NGC 7006	V54	4500	0.80	2.25	-1.65	-1.72	-0.54

Table 3—Continued

Association	Star	T_{eff} (K)	log g	v_t (km s ⁻¹)	[Fe/H] LIT ^a	[Fe/H]	[Mn/Fe]
NGC 7078 (M15)	K341	4275	0.45	2.00	-2.35	-2.46	-0.29
NGC 7078 (M15)	K387	4400	0.65	1.85	-2.42	-2.51	-0.38
NGC 7078 (M15)	K969	4625	1.30	2.60	-2.42	-2.56	-0.44
NGC 7078 (M15)	K431	4375	0.50	2.30	-2.43	-2.50	-0.39
NGC 7078 (M15)	K146	4450	0.80	1.90	-2.46	-2.58	-0.42
NGC 7078 (M15)	K386	4200	0.15	1.85	-2.43	-2.51	-0.45
NGC 7078 (M15)	K583	4275	0.30	1.90	-2.40	-2.51	-0.46
NGC 7078 (M15)	K702	4325	0.25	1.90	-2.44	-2.45	-0.44
NGC 7078 (M15)	K462	4225	0.30	1.85	-2.45	-2.48	-0.36
NGC 7078 (M15)	K490	4350	0.60	1.65	-2.44	-2.59	-0.06
NGC 7078 (M15)	K634	4225	0.30	1.85	-2.38	-2.44	-0.31
Pal 5	E	4500	1.45	1.65	-1.39	-1.63	-0.22
Pal 5	F	4500	1.50	1.60	-1.33	-1.43	-0.38
Pal 5	G	4535	1.55	1.55	-1.31	-1.43	-0.28
Pal 5	H	4750	1.55	1.70	-1.32	-1.53	-0.28
FIELD (JF)	171	5275	4.1	1.05	-1.00	-0.91	-0.27
FIELD (JF)	2413	5050	2.2	1.60	-1.96	-2.01	-0.38
FIELD (JF)	3026	5950	3.9	1.40	-1.32	-1.32	-0.24
FIELD (JF)	3086	5700	4.1	1.00	-0.17	-0.06	-0.29
FIELD (JF)	5336	5250	4.4	0.90	-0.98	-0.83	-0.32
FIELD (JF)	5445	5150	2.8	1.50	-1.58	-1.61	-0.32
FIELD (JF)	5458	4450	1.4	1.55	-1.04	-0.87	-0.33
FIELD (JF)	6710	4625	1.2	1.95	-1.83	-1.90	-0.28
FIELD (JF)	7217	5550	4.2	0.70	-0.48	-0.41	-0.36
FIELD (JF)	10140	5425	4.1	0.85	-1.14	-0.97	-0.41
FIELD (JF)	10449	5650	4.4	1.00	-0.98	-0.90	-0.43
FIELD (JF)	11349	5375	4.3	0.80	-0.29	-0.15	-0.22
FIELD (JF)	12306	5650	4.1	1.05	-0.63	-0.51	-0.35
FIELD (JF)	13366	5700	4.2	0.95	-0.77	-0.72	-0.33
FIELD (JF)	14086	5075	3.6	1.10	-0.71	-0.68	-0.32

Table 3—Continued

Association	Star	T_{eff} (K)	$\log g$	v_t (km s ⁻¹)	[Fe/H] LIT ^a	[Fe/H]	[Mn/Fe]
FIELD (JF)	15394	5150	3.4	1.00	-0.30	-0.08	-0.29
FIELD (JF)	16214	4825	2.0	1.45	-1.74	-1.72	-0.39
FIELD (JF)	17085	6500	4.2	1.70	-0.22	-0.13	-0.20
FIELD (JF)	17147	5800	4.3	1.10	-0.91	-0.83	-0.34
FIELD (JF)	17666	5050	4.5	0.60	-1.10	-0.93	-0.47
FIELD (JF)	18235	4950	3.2	0.90	-0.72	-0.63	-0.45
FIELD (JF)	18915	4700	4.8	1.35	-1.85	-1.77	-0.33
FIELD (JF)	18995	5575	2.2	2.05	-1.26	-1.24	-0.37
FIELD (JF)	19007	5150	4.5	1.20	-0.62	-0.51	-0.03
FIELD (JF)	19378	4500	1.2	1.70	-1.73	-1.75	-0.34
FIELD (JF)	21000	6200	4.1	1.40	-0.16	-0.11	-0.22
FIELD (JF)	21586	4850	4.1	0.25	-0.91	-0.67	-0.35
FIELD (JF)	21609	5200	3.8	1.55	-1.76	-1.70	-0.36
FIELD (JF)	21648	4300	0.4	1.70	-1.88	-1.84	-0.40
FIELD (JF)	21767	5650	4.5	0.70	-0.44	-0.35	-0.31
FIELD (JF)	22246	5200	4.5	1.20	-0.38	-0.33	-0.13
FIELD (JF)	22632	5825	4.3	1.35	-1.59	-1.61	-0.40
FIELD (JF)	26688	6500	4.1	1.50	-0.60	-0.61	-0.14
FIELD (JF)	27654	4550	2.1	1.50	-0.94	-0.87	-0.32
FIELD (JF)	28188	6175	4.6	1.25	-0.62	-0.63	-0.17
FIELD (JF)	30668	5150	3.1	1.05	-1.50	-1.54	-0.52
FIELD (JF)	30990	5825	4.0	1.30	-0.89	-0.93	-0.29
FIELD (JF)	31188	5750	4.1	1.65	-0.80	-0.63	-0.24
FIELD (JF)	31639	5300	4.3	0.60	-0.62	-0.47	-0.30
FIELD (JF)	32308	5175	4.1	1.00	-0.64	-0.42	-0.27
FIELD (JF)	33582	5725	4.3	1.25	-0.74	-0.80	-0.12
FIELD (JF)	34146	6300	4.2	1.95	-0.40	-0.43	-0.16
FIELD (JF)	34548	6250	4.5	1.40	-0.46	-0.45	-0.12
FIELD (JF)	36491	5800	4.4	1.10	-0.93	-0.87	-0.31
FIELD (JF)	36849	5850	4.1	1.10	-0.88	-0.88	-0.27

Table 3—Continued

Association	Star	T_{eff} (K)	$\log g$	v_t (km s ⁻¹)	[Fe/H] LIT ^a	[Fe/H]	[Mn/Fe]
FIELD (JF)	38541	5300	4.7	0.85	-1.79	-1.74	-0.50
FIELD (JF)	38621	4700	1.7	2.25	-1.81	-1.88	-0.26
FIELD (JF)	38625	5200	4.4	0.30	-0.86	-0.73	-0.34
FIELD (JF)	40068	5225	3.0	1.35	-2.05	-1.98	-0.40
FIELD (JF)	44075	5900	4.2	1.25	-0.91	-0.90	-0.29
FIELD (JF)	44116	6275	4.1	1.45	-0.58	-0.53	-0.23
FIELD (JF)	44716	5000	2.1	1.70	-1.08	-1.10	-0.32
FIELD (JF)	44919	6350	3.8	1.80	-0.65	-0.68	-0.08
FIELD (JF)	47139	4600	1.3	1.80	-1.46	-1.48	-0.38
FIELD (JF)	47640	6600	4.4	1.50	-0.08	-0.05	-0.24
FIELD (JF)	48146	6200	4.6	1.05	-0.05	-0.02	-0.19
FIELD (JF)	49371	4950	2.3	1.75	-1.95	-1.89	-0.38
FIELD (JF)	50139	5600	4.3	0.35	-0.68	-0.56	-0.31
FIELD (JF)	54858	5250	2.0	2.15	-1.17	-1.20	-0.34
FIELD (JF)	57265	5875	4.0	1.50	-1.10	-1.05	-0.36
FIELD (JF)	57850	4375	0.8	2.75	-1.78	-1.78	-0.29
FIELD (JF)	58229	5875	4.1	1.25	-0.94	-0.92	-0.43
FIELD (JF)	58357	5050	3.4	1.20	-0.65	-0.72	-0.25
FIELD (JF)	59239	5125	2.1	1.55	-1.49	-1.50	-0.39
FIELD (JF)	59330	5750	4.1	1.25	-0.75	-0.73	-0.26
FIELD (JF)	59750	6200	4.4	1.10	-0.78	-0.64	-0.45
FIELD (JF)	60551	5725	4.4	1.05	-0.86	-0.87	-0.24
FIELD (JF)	62747	4285	2.2	1.45	-1.54	-1.51	-0.45
FIELD (JF)	62882	5600	3.7	0.04	-1.26	-1.12	-0.55
FIELD (JF)	63970	6075	4.4	1.00	-0.09	0.03	-0.26
FIELD (JF)	64115	4650	2.4	1.10	-0.74	-0.62	-0.48
FIELD (JF)	64426	5800	4.1	1.25	-0.82	-0.78	-0.30
FIELD (JF)	65268	6250	4.1	1.50	-0.67	-0.60	-0.23
FIELD (JF)	66246	4400	1.0	2.55	-1.91	-2.00	-0.19
FIELD (JF)	66509	5350	4.2	0.60	-0.68	-0.53	-0.43

Table 3—Continued

Association	Star	T_{eff} (K)	$\log g$	v_t (km s ⁻¹)	[Fe/H] LIT ^a	[Fe/H]	[Mn/Fe]
FIELD (JF)	66665	5500	3.8	1.05	-0.97	-0.78	-0.48
FIELD (JF)	66815	5875	4.5	0.95	-0.64	-0.63	-0.26
FIELD (JF)	68796	5725	4.5	0.90	-0.52	-0.43	-0.24
FIELD (JF)	68807	4575	1.1	1.90	-1.83	-1.82	-0.33
FIELD (JF)	70681	5450	4.5	0.80	-1.25	-1.23	-0.38
FIELD (JF)	71886	6400	4.1	1.50	-0.40	-0.32	-0.24
FIELD (JF)	71887	6100	4.3	1.20	-0.49	-0.45	-0.26
FIELD (JF)	71939	6300	4.4	1.50	-0.37	-0.36	-0.18
FIELD (JF)	73385	5575	3.6	1.35	-1.59	-1.59	-0.31
FIELD (JF)	73960	4500	1.4	2.10	-1.37	-1.33	-0.38
FIELD (JF)	74033	5675	4.1	1.05	-0.78	-0.80	-0.38
FIELD (JF)	74067	5575	4.3	1.10	-0.90	-0.88	-0.28
FIELD (JF)	74079	5825	4.0	1.30	-0.83	-0.75	-0.31
FIELD (JF)	74234	4750	4.5	0.70	-1.51	-1.33	-0.51
FIELD (JF)	74235	4850	4.5	0.70	-1.57	-1.42	-0.47
FIELD (JF)	80837	5800	4.1	1.15	-0.83	-0.74	-0.37
FIELD (JF)	81170	5175	4.7	0.30	-1.26	-1.23	-0.38
FIELD (JF)	81461	5600	4.1	1.20	-0.65	-0.46	-0.31
FIELD (JF)	85007	5900	4.2	1.20	-0.50	-0.38	-0.34
FIELD (JF)	85378	5625	4.0	1.10	-0.64	-0.53	-0.35
FIELD (JF)	85757	5450	3.8	1.05	-0.76	-0.65	-0.35
FIELD (JF)	86013	5750	4.4	1.15	-0.82	-0.84	-0.25
FIELD (JF)	86431	5675	4.1	1.15	-0.64	-0.54	-0.37
FIELD (JF)	88010	5200	4.0	0.70	-1.49	-1.41	-0.38
FIELD (JF)	88039	5700	4.0	1.30	-0.96	-0.88	-0.33
FIELD (JF)	91058	6025	4.1	1.40	-0.54	-0.49	-0.22
FIELD (JF)	92167	4575	2.4	1.40	-1.47	-1.80	-0.51
FIELD (JF)	92532	5825	4.3	1.00	-0.56	-0.44	-0.25
FIELD (JF)	92781	5650	4.2	0.95	-0.75	-0.57	-0.48
FIELD (JF)	94449	5625	3.7	1.15	-1.26	-1.22	-0.34

Table 3—Continued

Association	Star	T_{eff} (K)	$\log g$	v_t (km s ⁻¹)	[Fe/H] LIT ^a	[Fe/H]	[Mn/Fe]
FIELD (JF)	96185	5700	4.1	1.00	-0.58	-0.53	-0.35
FIELD (JF)	97023	5800	3.8	1.30	-0.48	-0.35	-0.27
FIELD (JF)	97468	4450	1.1	1.90	-1.71	-1.73	-0.32
FIELD (JF)	98020	5325	4.6	1.10	-1.67	-1.58	-0.49
FIELD (JF)	98532	5550	3.6	1.30	-1.23	-1.18	-0.33
FIELD (JF)	99423	5650	3.8	1.30	-1.50	-1.43	-0.43
FIELD (JF)	99938	5650	4.0	1.20	-0.74	-0.65	-0.31
FIELD (JF)	100568	5650	4.4	1.10	-1.17	-1.12	-0.36
FIELD (JF)	100792	5875	4.2	1.40	-1.23	-1.19	-0.34
FIELD (JF)	101346	6000	3.9	1.40	-0.65	-0.68	-0.14
FIELD (JF)	101382	5125	4.0	0.40	-0.66	-0.38	-0.39
FIELD (JF)	103269	5300	4.6	0.85	-1.81	-1.80	-0.48
FIELD (JF)	104659	5825	4.3	1.00	-1.12	-1.03	-0.38
FIELD (JF)	104660	5500	3.9	1.15	-0.96	-0.78	-0.41
FIELD (JF)	105888	5700	4.3	1.00	-0.75	-0.63	-0.34
FIELD (JF)	107975	6275	3.9	1.50	-0.64	-0.54	-0.33
FIELD (JF)	109067	5300	4.3	0.85	-0.97	-0.88	-0.37
FIELD (JF)	109390	4800	2.2	1.50	-1.34	-1.33	-0.43
FIELD (JF)	112796	4525	1.0	2.85	-2.25	-2.26	-0.16
FIELD (JF)	114962	5825	4.3	1.40	-1.54	-1.33	-0.44
FIELD (JF)	115610	4800	4.1	1.20	-0.63	-0.35	-0.13
FIELD (JF)	115949	4500	0.9	2.75	-2.19	-2.17	-0.28
FIELD (JF)	116082	6275	3.7	1.60	-0.82	-0.80	-0.22
FIELD (JF)	117029	5425	3.8	1.05	-0.81	-0.75	-0.30
FIELD (JF)	117041	5300	4.2	0.90	-0.88	-0.81	-0.25
FIELD (JS)	B-010306	5550	4.19	1.50	-1.13	-1.10	-0.30
FIELD (JS)	B-012582	5148	2.86	1.20	-2.21	-2.26	-0.41
FIELD (JS)	B+191185	5500	4.19	1.10	-1.09	-1.09	-0.31
FIELD (JS)	B+521601	4911	2.10	2.05	-1.40	-1.49	-0.33
FIELD (JS)	G005-001	5500	4.32	0.80	-1.24	-1.18	-0.31

Table 3—Continued

Association	Star	T_{eff} (K)	$\log g$	v_t (km s ⁻¹)	[Fe/H] LIT ^a	[Fe/H]	[Mn/Fe]
FIELD (JS)	G009-036	5625	4.57	0.65	-1.17	-1.17	-0.44
FIELD (JS)	G017-025	4966	4.26	0.80	-1.54	-1.37	-0.42
FIELD (JS)	G023-014	5025	3.00	1.30	-1.64	-1.57	-0.44
FIELD (JS)	G028-043	5061	4.50	0.80	-1.64	-1.58	-0.42
FIELD (JS)	G029-025	5225	4.28	0.80	-1.09	-0.91	-0.44
FIELD (JS)	G040-008	5200	4.08	0.50	-0.97	-0.80	-0.37
FIELD (JS)	G058-025	6001	4.21	1.05	-1.40	-1.49	-0.36
FIELD (JS)	G059-001	5922	3.98	0.40	-0.95	-0.76	-0.38
FIELD (JS)	G063-046	5705	4.25	1.30	-0.90	-0.85	-0.28
FIELD (JS)	G068-003	4975	3.50	0.95	-0.76	-0.65	-0.28
FIELD (JS)	G074-005	5668	4.24	1.50	-1.05	-1.03	-0.28
FIELD (JS)	G090-025	5303	4.46	1.20	-1.78	-1.83	-0.53
FIELD (JS)	G095-57A	4965	4.40	0.90	-1.22	-1.08	-0.37
FIELD (JS)	G095-57B	4800	4.57	0.60	-1.06	-1.03	-0.30
FIELD (JS)	G102-020	5254	4.44	0.90	-1.25	-1.23	-0.32
FIELD (JS)	G102-027	5600	3.75	1.05	-0.59	-0.50	-0.35
FIELD (JS)	G113-022	5525	4.25	1.10	-1.18	-1.19	-0.40
FIELD (JS)	G122-051	4864	4.51	1.40	-1.43	-1.42	-0.43
FIELD (JS)	G123-009	5487	4.75	1.50	-1.25	-1.30	-0.29
FIELD (JS)	G126-036	5487	4.50	0.60	-1.06	-0.96	-0.36
FIELD (JS)	G126-062	5941	3.98	2.00	-1.59	-1.75	-0.28
FIELD (JS)	G140-046	4980	4.42	0.70	-1.30	-1.18	-0.43
FIELD (JS)	G153-021	5700	4.36	1.40	-0.70	-0.71	-0.18
FIELD (JS)	G176-053	5593	4.50	1.20	-1.34	-1.41	-0.37
FIELD (JS)	G179-022	5082	3.20	1.20	-1.35	-1.28	-0.40
FIELD (JS)	G180-024	6059	4.09	0.50	-1.34	-1.38	-0.28
FIELD (JS)	G188-022	5827	4.27	1.20	-1.52	-1.48	-0.36
FIELD (JS)	G191-055	5770	4.50	1.00	-1.63	-1.77	-0.19
FIELD (JS)	G192-043	6085	4.50	1.50	-1.50	-1.56	-0.33
FIELD (JS)	G221-007	5016	3.37	0.90	-0.98	-0.86	-0.33

Table 3—Continued

Association	Star	T_{eff} (K)	log g	v_t (km s ⁻¹)	[Fe/H] LIT ^a	[Fe/H]	[Mn/Fe]
FIELD (JS)	2665	4990	2.34	2.00	-1.99	-2.17	-0.38
FIELD (JS)	3008	4250	0.25	2.60	-2.08	-2.14	-0.33
FIELD (JS)	6755	5105	2.93	2.50	-1.68	-1.78	-0.29
FIELD (JS)	8724	4535	1.40	1.40	-1.91	-1.79	-0.51
FIELD (JS)	21581	4870	2.27	1.40	-1.71	-1.75	-0.43
FIELD (JS)	23798	4450	1.06	2.50	-2.26	-2.32	-0.29
FIELD (JS)	25329	4842	4.66	0.60	-1.67	-1.67	-0.40
FIELD (JS)	25532	5396	2.00	1.20	-1.34	-1.17	-0.50
FIELD (JS)	26297	4322	1.11	1.80	-1.98	-1.92	-0.41
FIELD (JS)	29574	4250	0.80	2.20	-2.00	-2.00	-0.43
FIELD (JS)	37828	4350	1.50	1.85	-1.62	-1.59	-0.40
FIELD (JS)	44007	4851	2.00	2.00	-1.72	-1.74	-0.39
FIELD (JS)	63791	4675	2.00	2.00	-1.90	-1.86	-0.39
FIELD (JS)	74462	4700	2.00	1.90	-1.52	-1.55	-0.29
FIELD (JS)	82590	6005	2.75	3.00	-1.50	-1.57	-0.30
FIELD (JS)	85773	4268	0.50	2.00	-2.62	-2.50	-0.29
FIELD (JS)	101063	5150	3.25	1.70	-1.33	-1.38	-0.31
FIELD (JS)	103036	4200	0.25	3.00	-2.04	-1.93	-0.48
FIELD (JS)	103545	4666	1.64	2.00	-2.45	-2.41	-0.38
FIELD (JS)	105546	5190	2.49	1.60	-1.48	-1.52	-0.25
FIELD (JS)	105755	5701	3.82	1.20	-0.83	-0.76	-0.30
FIELD (JS)	106516	6166	4.21	1.10	-0.81	-0.76	-0.38
FIELD (JS)	108317	5234	2.68	2.00	-2.18	-2.25	-0.17
FIELD (JS)	110184	4250	0.50	2.50	-2.72	-2.66	-0.32
FIELD (JS)	121135	4934	1.91	1.60	-1.54	-1.49	-0.50
FIELD (JS)	122563	4572	1.36	2.90	-2.72	-2.68	-0.25
FIELD (JS)	122956	4508	1.55	1.60	-1.95	-1.85	-0.44
FIELD (JS)	124358	4688	1.57	2.10	-1.91	-1.88	-0.40
FIELD (JS)	132475	5425	3.56	2.30	-1.86	-1.80	-0.37
FIELD (JS)	135148	4183	0.25	2.90	-2.17	-2.17	-0.25

Table 3—Continued

Association	Star	T_{eff} (K)	$\log g$	v_t (km s ⁻¹)	$[Fe/H]$ LIT ^a	$[Fe/H]$	$[Mn/Fe]$
FIELD (JS)	141531	4356	1.14	2.20	-1.79	-1.84	-0.33
FIELD (JS)	165195	4237	0.78	2.30	-2.60	-2.56	-0.43
FIELD (JS)	166161	5350	2.56	2.25	-1.23	-1.36	-0.33
FIELD (JS)	171496	4952	2.37	1.40	-0.67	-0.57	-0.33
FIELD (JS)	184266	6000	2.74	3.00	-1.43	-1.52	-0.30
FIELD (JS)	186478	4598	1.43	2.00	-2.56	-2.64	-0.48
FIELD (JS)	187111	4271	1.05	1.90	-1.97	-1.90	-0.40
FIELD (JS)	188510	5564	4.51	1.00	-1.32	-1.50	-0.43
FIELD (JS)	193901	5750	4.46	1.50	-1.08	-1.13	-0.36
FIELD (JS)	194598	6044	4.19	1.00	-1.08	-1.12	-0.37
FIELD (JS)	201891	5909	4.19	1.00	-1.09	-1.06	-0.37
FIELD (JS)	204543	4672	1.49	2.00	-1.87	-1.95	-0.40
FIELD (JS)	206739	4647	1.78	1.90	-1.72	-1.77	-0.30
FIELD (JS)	210295	4750	2.50	1.55	-1.46	-1.48	-0.41
FIELD (JS)	214362	5727	2.62	2.00	-1.87	-1.93	-0.50
FIELD (JS)	218857	5103	2.44	1.90	-1.90	-2.08	-0.28
FIELD (JS)	221170	4410	1.09	1.70	-2.35	-2.30	-0.38
FIELD (JS)	232078	3875	0.50	2.10	-1.69	-1.74	-0.50
FIELD (JS)	233666	5157	2.00	1.70	-1.79	-1.86	-0.22

Note. — The complete version of this table is in the electronic edition of the Journal. The printed edition contains only a sample.

^aAs discussed in text, literature values of $[Fe/H]$ are provided.

Note. — Field stars from the Fulbright (2000) survey (labeled as JF) have Hipparcos identifications. Similarly, target stars of the Simmerer et al. (2004) survey (designated as JS) have Henry Draper identifications unless otherwise indicated.

Table 4. External Data Source Stellar Model Parameters and Individual [Fe/H] and [Mn/Fe] Values

Association	Star	T_{eff} (K)	$\log g$	v_t (km s^{-1})	[Fe/H] LIT ^a	[Fe/H]	[Mn/Fe]
Cr 261	1045	4400	1.50	1.20	−0.16	−0.14	−0.41
Cr 261	1080	4490	2.20	1.20	−0.11	−0.25	−0.45
Cr 261	1871	4000	0.70	1.50	−0.31	−0.59	−0.22
Cr 261	2105	4300	1.50	1.50	−0.32	−0.47	−0.21
NGC 288	20	4050	0.60	1.75	−1.44	−1.62	−0.31
NGC 288	231	4300	1.10	1.50	−1.41	−1.50	−0.32
NGC 288	245	4250	0.80	1.40	−1.41	−1.47	−0.30
NGC 288	274	4025	0.70	1.90	−1.37	−1.48	−0.33
NGC 288	281	4125	0.60	1.71	−1.42	−1.65	−0.29
NGC 288	287	4350	1.20	1.40	−1.45	−1.34	−0.44
NGC 288	297	4330	1.20	1.70	−1.41	−1.62	−0.23
NGC 288	307	4350	1.20	1.35	−1.40	−1.63	−0.24
NGC 288	338	4325	1.30	1.60	−1.37	−1.55	−0.28
NGC 288	344	4180	0.80	1.60	−1.36	−1.45	−0.32
NGC 288	351	4330	1.20	1.55	−1.30	−1.53	−0.36
NGC 288	403	3950	0.20	1.90	−1.43	−1.59	−0.32
NGC 288	531	3780	0.10	1.60	−1.31	−1.70	−0.42
NGC 362	1137	4000	0.70	2.00	−1.37	−1.51	−0.31
NGC 362	1159	4125	0.80	1.90	−1.27	−1.37	−0.34
NGC 362	1334	3975	0.40	1.95	−1.30	−1.37	−0.42
NGC 362	1401	3875	0.00	1.90	−1.32	−1.39	−0.34
NGC 362	1423	3950	0.10	2.35	−1.37	−1.42	−0.41
NGC 362	1441	3975	0.20	1.90	−1.31	−1.44	−0.29
NGC 362	2115	3900	0.00	2.30	−1.38	−1.49	−0.32
NGC 362	2127	4110	0.60	2.25	−1.30	−1.52	−0.39
NGC 362	2423	4000	0.40	1.85	−1.32	−1.42	−0.41
NGC 362	77	4075	0.20	2.50	−1.34	−1.41	−0.34
NGC 362	MB2	4100	0.60	2.25	−1.30	−1.58	−0.20
NGC 362	V2	3950	0.10	2.70	−1.30	−1.58	−0.48
NGC 3201	5	4750	1.80	1.70	−1.38	−1.53	−0.42

Table 4—Continued

Association	Star	T_{eff} (K)	log g	v_t (km s ⁻¹)	[Fe/H] LIT ^a	[Fe/H]	[Mn/Fe]
NGC 3201	8	4410	1.50	1.80	-1.17	-1.56	-0.28
NGC 3201	9	4600	1.90	1.70	-1.18	-1.45	-0.34
NGC 3201	42	4500	1.50	2.00	-1.32	-1.65	-0.29
NGC 3201	112	4350	1.30	1.60	-1.38	-1.64	-0.18
NGC 3201	121	4000	0.00	2.00	-1.40	-1.56	-0.42
NGC 3201	168	4100	0.20	1.80	-1.42	-1.61	-0.30
NGC 3201	238	4250	0.90	1.80	-1.42	-1.53	-0.44
NGC 3201	293	4250	1.20	1.80	-1.39	-1.56	-0.38
NGC 3201	301	4250	1.00	2.20	-1.49	-1.65	-0.33
NGC 3201	312	4250	0.70	1.80	-1.47	-1.49	-0.49
NGC 3201	318	4350	0.80	1.90	-1.52	-1.59	-0.39
NGC 3201	357	4150	0.70	2.00	-1.55	-1.78	-0.21
NGC 3201	419	4500	1.20	1.70	-1.28	-1.40	-0.58
NGC 6287	1491	4375	1.00	1.75	-2.15	-2.28	-0.30
NGC 6287	1387	4250	0.80	1.90	-2.10	-2.33	-0.26
NGC 6293	2673	4250	0.50	1.90	-2.16	-2.24	-0.35
NGC 6293	3857	4450	0.70	1.75	-2.18	-2.40	-0.39
NGC 6528	I-42	4200	1.60	1.20	-0.14	-0.34	-0.23
NGC 6528	I-36	4300	1.50	1.50	-0.13	-0.37	-0.21
NGC 6528	I-18	4800	2.00	1.50	-0.05	-0.03	-0.33
NGC 6541	I-44	4250	0.70	1.85	-1.85	-1.95	-0.28
NGC 6541	II-113	4200	0.50	1.80	-1.86	-1.91	-0.36
NGC 6705 (M11)	660	4500	1.50	2.00	0.05	0.03	-0.43
NGC 6705 (M11)	669	4500	1.40	2.00	0.09	0.18	-0.32
NGC 6705 (M11)	686	4600	2.00	2.00	0.13	0.13	-0.45
NGC 6705 (M11)	779	4250	1.60	2.50	-0.01	-0.07	-0.49
NGC 6705 (M11)	916	4500	1.30	2.00	0.01	-0.04	-0.34
NGC 6705 (M11)	926	4500	1.50	2.00	-0.21	-0.59	-0.38
NGC 6705 (M11)	1184	4600	2.20	2.00	0.24	0.24	-0.30
NGC 6705 (M11)	1223	4750	2.50	2.00	0.19	-0.06	-0.39

Table 4—Continued

Association	Star	T_{eff} (K)	$\log g$	v_t (km s ⁻¹)	[Fe/H] LIT ^a	[Fe/H]	[Mn/Fe]
NGC 6705 (M11)	1256	4600	2.50	2.00	0.31	0.28	-0.17
NGC 6705 (M11)	1423	4750	2.90	2.50	0.21	0.04	-0.05
NGC 6752	1	4749	1.95	1.41	-1.58	-1.69	-0.43
NGC 6752	2	4779	1.98	1.39	-1.59	-1.69	-0.48
NGC 6752	3	4796	2.03	1.42	-1.64	-1.74	-0.39
NGC 6752	4	4806	2.04	1.40	-1.61	-1.66	-0.46
NGC 6752	6	4804	2.06	1.40	-1.61	-1.87	-0.38
NGC 6752	7	4829	2.10	1.33	-1.84	-1.74	-0.53
NGC 6752	8	4910	2.15	1.33	-1.62	-1.60	-0.43
NGC 6752	9	4824	2.11	1.38	-1.63	-1.72	-0.41
NGC 6752	10	4836	2.13	1.37	-1.60	-1.63	-0.52
NGC 6752	11	4829	2.13	1.32	-1.64	-1.65	-0.47
NGC 6752	12	4841	2.15	1.34	-1.62	-1.72	-0.40
NGC 6752	15	4850	2.19	1.35	-1.61	-1.75	-0.45
NGC 6752	16	4906	2.24	1.32	-1.60	-1.73	-0.44
NGC 6752	19	4928	2.32	1.29	-1.61	-1.75	-0.49
NGC 6752	20	4929	2.33	1.32	-1.59	-1.69	-0.48
Pal 12	S1	3900	0.63	1.80	-0.76	-0.81	-0.31
Pal 12	1118	4000	0.84	1.80	-0.80	-0.82	-0.35
Pal 12	1128	4260	1.30	1.70	-0.82	-0.84	-0.40
Pal 12	1305	4465	1.62	1.70	-0.80	-0.84	-0.38

Note. — The complete version of this table is in the electronic edition of the Journal. The printed edition contains only a sample.

^aAs discussed in text, literature values of [Fe/H] are provided.

Table 5. Line Parameters

Element	λ [\AA]	χ [eV]	$\log(gf)$	$E\gamma$
Fe I	6024.06	4.545	0.040	2.2
Fe I	6027.05	4.073	−1.089	2.0
Mn I	6013.51	3.070	−0.251	1.5
Mn I	6016.64	3.071	−0.216	1.5
Mn I	6021.82	3.073	0.034	1.5

Table 6. LTG Cluster Mean Abundances

Cluster	N_{Stars}	$\langle[Fe/H]\rangle$	σ	$\langle[Fe/H]\rangle_{LIT}$	σ	$[Fe/H]_{AVG}$ ^a	$\langle[Mn/Fe]\rangle$	σ	$\langle[Mn/Fe]\rangle_{AVG}$ ^b
NGC 5272 (M3)	20	−1.59	0.08	−1.59	0.07	−1.59	−0.43	0.09	−0.43
NGC 5904 (M5)	31	−1.37	0.11	−1.34	0.08	−1.35	−0.40	0.08	−0.41
NGC 6121 (M4)	20	−1.24	0.06	−1.19	0.02	−1.21	−0.39	0.07	−0.42
NGC 6205 (M13)	17	−1.67	0.06	−1.60	0.05	−1.64	−0.38	0.04	−0.41
NGC 6254 (M10)	12	−1.64	0.11	−1.53	0.09	−1.58	−0.38	0.08	−0.43
NGC 6341 (M92)	4	−2.45	0.05	−2.27	0.04	−2.36	−0.37	0.05	−0.45
NGC 6838 (M71)	10	−1.13	0.15	−0.79	0.05	−0.96	−0.16	0.14	−0.32
NGC 7006	6	−1.62	0.11	−1.59	0.04	−1.60	−0.42	0.07	−0.43
NGC 7078 (M15)	11	−2.51	0.05	−2.42	0.03	−2.46	−0.36	0.12	−0.40
Pal 5	4	−1.51	0.10	−1.34	0.04	−1.42	−0.29	0.07	−0.36

^aThese values are the average of the $[Fe\ I/H]$ values from this study and literature.

^bThese values are computed using $[Fe/H](AVG)$.